

A Thesis on

Enhancement of Heat Removal Rate in Film Boiling Regime by Spray Cooling with Sea Water

Submitted to
National Institute of Technology, Rourkela
for the partial fulfilment of the requirement

of

Master of Technology

in

Chemical Engineering

By

Akash Ranjan Pati

(Roll No:214CH1551)

Under the guidance

of

Dr. Soumya Sanjeeb Mohapatra



DEPARTMENT OF CHEMICAL ENGINEERING
NATIONAL INSTITUTE OF TECHNOLOGY, ROURKELA
MAY-2016

DEPARTMENT OF CHEMICAL ENGINEERING
NATIONAL INSTITUTE OF TECHNOLOGY
ROURKELA



Supervisor's Certificate

This is to certify that the thesis entitled “*Enhancement of Heat Removal Rate in Film Boiling Regime by Spray Cooling with Sea Water*” submitted by **Akash Ranjan Pati** to National Institute of Technology, Rourkela is a record of bona fide research work under my supervision.

Dr. Soumya Sanjeeb Mohapatra

Department of Chemical Engineering

National Institute of Technology, Rourkela

Acknowledgement

In pursuit of this academic endeavor, I feel that I have been singularly fortunate; inspiration, guidance, direction, co-operation, love and care all came in my way in abundance and it seems almost an impossible task to acknowledge the same in adequate terms. Yes, I shall be failing in my duty if I do not record my profound sense of indebtedness and heartfelt gratitude to my guide **Dr. Soumya Sanjeeb Mohapatra** who guided me in pursuance of this work. His association will remain a beacon light to me throughout my career.

I also express my sincere gratitude to **Prof. A. Sahoo, Project Coordinator** of Department of Chemical Engineering and **Prof. Dr. P. Rath, Head of the Department** of Chemical Engineering, National Institute of Technology, Rourkela, for their valuable guidance and timely suggestions during the entire duration of my project work. I would like to extend my sincere thanks to my friends Dheeraj and Bhatt for their unconditional encouragement, for the stimulating discussions, and also to my seniors Lily, Sourav and Saroj for sincere help extended in completion of my project. I would like to express my gratitude towards **Prof. B. Munshi, Prof. S. Paria** and **Prof. M. Kundu** for their support and encouragement. Last but not the least, I wish to profoundly acknowledge my family for their constant support.

Date:

Akash Ranjan Pati
Roll No- 214CH1551

Declaration of Originality

I Akash Ranjan Pati, Roll Number 214CH1551, hereby declare that the thesis entitled **“Enhancement of Heat Removal Rate in Film Boiling Regime by Spray Cooling with Sea Water”** presents my original work carried out as a M.Tech student of NIT Rourkela and, to the best of my knowledge, contains no material previously published or written by another person, nor any material presented by me for the award of any degree or diploma of NIT Rourkela or any other institution. Any contribution made to this research by others, with whom I have worked at NIT Rourkela or elsewhere, is explicitly acknowledged in the thesis. Works of other authors cited in this thesis have been duly acknowledged under the sections “References”. I have also submitted my original research records to the scrutiny committee for evaluation of my thesis. I am fully aware that in case of any non-compliance detected in future, the Senate of NIT Rourkela may withdraw the degree awarded to me on the basis of the present thesis.

May 26, 2016

NIT Rourkela

Akash Ranjan Pati

Abstract

Water spray cooling is an important technology which is used in steel industries. The final mechanical properties of the steel are directly proportional to the quenching rate. Spray cooling is an important technique to achieve very high cooling rate. However, the achieved cooling rate is not sufficient for the metal which are used in some specific applications such as production of low weight and high strength steel which is used for the fabrication of light weight vehicle. Hence, the current process needs to be further enhanced. In the current case, experiments were conducted by using spray of different coolants such as pure water, salt added water surfactant added water, salt plus surfactant added water and sea water. For the above mentioned experiments an experimental set up was fabricated and for the calculation INTEMP software has been used. Initially, for the coolants, the optimum height (40 mm) and the flow rate ($16.67 \times 10^{-5} \text{ m}^3/\text{s}$) were determined. The experimental result of salt added spray cooling reveals that the quenching rate increases with increase in salt concentration up to 0.4 M due to salt deposition effect which alter the heat transfer mechanism from convection mode to conductive mode. However, further increment shows decline trend and this is due to the decrement of resultant thermal conductivity of the substrate. In addition to the above, cooling experiments also done by using sea water. The results show that the cooling rate increases with the increase in dilution and this happens because of the combined effect of salt deposition and contact angle decrement. In addition to the above, for the comparative study, among all the coolants, a cooling experiment was conducted with surfactant (Tween 20). Finally, the comparison among all the coolants has been made and from the comparison it is concluded that 100 % sea water produce maximum cooling rate.

Key words: quenching, salt deposition, enhancement, conduction

Contents

	Page No.
Abstract	I
List of Figures	IV
List of Tables	VII
1 Introduction and Literature Review	
1.1 Introduction	1
1.2 Literature review	3
2 Experimental Setup and Characterization	
2.1 Experimental setup and procedure	5
2.2 Calculation of surface heat flux and surface temperature by “INTEMP” software	6
2.3 Spray Characterization	8
2.3.1 Impingement density	8
2.3.2 Droplet velocity	9
2.3.3 Droplet diameter	10
2.3.4 Spray pressure	10
2.4 Material Characterization	11
2.5 Solution Characterization	12
2.5.1 Contact angle	12
2.5.2 Specific heat capacity, thermal conductivity and diffusivity	13
3 Results and Discussion	
3.1 Spray Cooling with Pure Water	15
3.1.1 Effect of nozzle height	15
3.1.2 Effect of water flow rate	16

3.2 Salt Added Spray Cooling	22
3.2.1 Effect of salt added water	23
3.3 Surfactant Added Spray Cooling	30
3.3.1 Effect of surfactant added water	30
3.4 Sea Water Added Spray Cooling	33
3.4.1 Effect of sea water on spray cooling	33
3.5 Comparative Study	39
3.6 Comparison with Previous Work	39
3.7 Validation	40
3.8 Measurement Uncertainty	41
4 Conclusions and Future work	
4.1 Conclusions	42
4.2 Future work	42
References	43

List of Figures

Figure No.		Page No.
Fig. 2.1	Schematic diagram of the experimental setup	6
Fig. 2.2	Computational domain of the steel plate	7
Fig. 2.3(a)	Photograph of the Patternator (top view)	8
Fig. 2.3(b)	Photograph of the Patternator (side view)	8
Fig. 2.4	Variation of local impingement density with varying water flow rate	9
Fig. 2.5	Variation of droplet mean velocity with liquid flow rate	9
Fig. 2.6	Variation of droplet diameter with liquid flow rate	10
Fig. 2.7	Variation of spray pressure with liquid flow rate	11
Fig. 2.8	Variation of contact angle with salt concentration	12
Fig. 2.9	Variation of contact angle with sea water concentration	13
Fig. 2.10	Variation of specific heat capacity with salt concentration	13
Fig. 2.11	Variation of thermal conductivity with salt concentration	14
Fig. 2.12	Variation of diffusivity with salt concentration	14
Fig. 3.1	Variation of surface heat flux with time	15
Fig. 3.2	Variation of sub surface temperature with time	16
Fig. 3.3	Variation of surface heat flux with time	17
Fig. 3.4	Variation of surface heat flux with surface temperature	18
Fig. 3.5(a)	Schematic diagram in case of low momentum droplet evaporation	19
Fig. 3.5(b)	Schematic diagram in case of high momentum droplet	19
Fig. 3.6	Variation of average heat flux with different water flow rates	19
Fig. 3.7	Variation of average cooling with different water flow rates	20
Fig. 3.8	Visual observation of experiments conducted at different flow rates	21

Fig. 3.9	Variation of dark zone diameter with time	22
Fig. 3.10	Variation of sub surface temperature with time	23
Fig. 3.11	Variation of surface heat flux with time	23
Fig. 3.12	Schematic diagram showing the mechanism of salt deposition	24
Fig. 3.13(a)	Schematic diagram of spray evaporative cooling by pure water	25
Fig. 3.13(b)	Schematic diagram of spray evaporative cooling by 0.4M salt solution	25
Fig. 3.13(c)	Schematic diagram of spray evaporative cooling by 0.6M salt solution	25
Fig. 3.14(a)	Microscopic images of steel plate	26
Fig. 3.14(b)	Microscopic images of steel plate after cooling with 0.1M salt solution	26
Fig. 3.14(c)	Microscopic images of steel plate after cooling with 0.4M salt solution	26
Fig. 3.14(d)	Microscopic images of steel plate after cooling with 0.6M salt solution	26
Fig. 3.15	Variation of Surface heat flux with surface temperature	27
Fig. 3.16	Variation of average heat flux with salt concentration	28
Fig. 3.17	Variation of average cooling rate with salt concentration	28
Fig. 3.18	Visual analysis of the experiments conducted with different salt solutions	29
Fig. 3.19	Variation of dark zone diameter with time	30
Fig. 3.20	Variation of temperature with time	31
Fig. 3.21	Variation of surface heat flux with time	31
Fig. 3.22	Variation of surface heat flux with surface temperature	32
Fig. 3.23(a)	Schematic diagram of spray cooling with pure water	32
Fig. 3.23(b)	Schematic diagram of spray cooling with surfactant added water	32
Fig. 3.24	Variation of temperature with time	33
Fig. 3.25	Variation of surface heat flux with time	34
Fig. 3.26(a)	Schematic diagram of spray cooling by water with salt	35
Fig. 3.26(b)	Schematic diagram of spray cooling with sea water	35

Fig. 3.27	Variation of surface heat flux with surface temperature	35
Fig. 3.28	Variation of average heat flux with sea water concentration	36
Fig. 3.29	Variation of average cooling rate with sea water concentration	36
Fig. 3.30	Microscopic image of the steel plate after cooling with 100 % sea water	37
Fig. 3.31	Variation of dark zone diameter with time	37
Fig. 3.32	Visual analysis of experiments conducted with different conc. of sea water	38
Fig. 3.33	Comparative study	39
Fig. 3.34	Variation of surface heat flux with cooling rate	40
Fig. 3.35	Validation of estimated temperature with the measured	40

List of Tables

Table No.		Page No.
Table 2.1	Composition of the material used in the experimentations	11
Table 2.2	Material properties	12
Table 3.1	Variation of nozzle height with spray area and average heat flux	16
Table 3.2	Amount of salt deposited on the steel plate	26

Chapter 1

Introduction and literature review

1.1 Introduction

High temperature cooling technologies such as cooling of electronic components, nuclear power plant, the use of powerful lasers, and different metallurgical processes, require much attention due to its high importance in the current society. Especially, in steel industry, spray cooling is used in strip casting and hot rolling on run-out table (ROT). For the aforesaid applications, the initial temperature ranges are considered from 800-1100 °C. In such cooling operations, a major set-back is the occurrence of early film-boiling or Leidenfrost phenomenon which declines the heat transfer rates.

The production of the materials for the aforesaid applications mainly depend on the material properties which are achieved during the cooling. Particularly, high tensile strength steel and moderate hardenability steel can be produced by increasing fineness of martensite lath [1] which is controlled by the heat removal rate in the temperature range of 600-900 °C [2].

Spray cooling produces better heat transfer rate when it is compared with conventional jet cooling. The main drawback of spray cooling is that it uniformly cools a large surface and removes larger amount of heat. On comparison with air atomized spray, it is found that it is cost effective process. However, the produced quenching rates by the spray are not sufficient for the above mentioned applications. For the aforesaid applications, high cooling rate is the essential criteria. For the production of high cooling rate, this cooling methodology needs to be further enhanced.

During the spray cooling, the liquid is broken into fine droplets and impinge individually on the hot surface [3]. The impingement of the water droplet improves the uniformity of the heat removal. During the spray cooling, the Leidenfrost affect appears at very low surface temperatures and due to this a vapor layer covers the plate surface. As a consequence, the heat transfer occurs from the hot plate to the water droplet by convection and this mode is not the suitable mode for high heat application. Hence, the main problem with the spray cooling is its low cooling rate [4,5].

Furthermore, by changing the heat transfer mode from convective to conductive, the heat transfer rate can be enhanced. The information reported in the open literature corroborates the aforesaid statement.

Available literature reveals that many researchers worked on the enhancement of spray cooling [7-9]. The literature also reveals that the presence of salt in water increases the spray cooling due to the change of heat transfer mode from convective mode to the conductive mode. But, all the reported information is at very low substrate temperatures which are not suitable for the above mentioned applications. Furthermore, it is also reported that the presence of surfactant also increases the heat removal rate of spray cooling. The presence of surfactant in water droplets during spray offer higher heat transfer area. However, the said works have been reported at very low temperatures. At high temperature, the effect of surfactant and salt have not been studied so far. Furthermore, no attempt has been made till date to enhance the spray cooling at high initial surface temperatures by using above mentioned additives.

From the aforesaid argument, it can be concluded that both the additives individually enhance the heat removal rate in the film boiling regime and hence in the proposed work, by utilizing the combined effects of the aforesaid additives (salt + surfactant), the spray has been further enhanced. This is achieved by using sea water in place of a mixture of salt and surfactant added water. The sea water exhibits both the characteristics of salt added water and surfactant added water. Hence, in the current work, an attempt has been made to enhance the spray cooling in the film boiling regime by using sea water.

In the current work, for the experimentation, a spray cooling experimental setup was fabricated. Experiments were conducted for different types of coolant such as pure water, surfactant added water, salt added water, surfactant and salt added water and finally with the sea water. After experimentation, by using INTEMP, the heat flux and surface temperatures were calculated. Initially, the optimum height and the optimum flow rate were determined and at these conditions experiments were conducted with different coolant concentrations. The result reveals that 100 % sea water produces the best cooling rate which is almost twice that of pure water.

1.2 Literature review

In the absence of any literature on spray cooling enhancement at high initial surface temperatures (900 °C) with very high mass flux in the open literature, the most relevant information has been discussed below. According to the literature at low temperature, the researchers have tried to enhance the spray cooling.

The reported information by Morgan et. al confirms that heat transfer rate enhance by mixing surfactants in evaporating liquids [10]. In the follow of research, the researchers noticed that heat removal rate increases in nucleate boiling duo to the addition of surfactant in evaporating water droplets. [11] Furthermore, the work done reveals that addition of surfactants in water droplet increases the viscosity and this may be another reason for boiling heat transfer rate enhancement [12]. The most relevant information reported by Chandra et. al. is based on spray cooling with surfactant [13]. In this study, the researched consider substrate surface temperature up to 240 °C. They found that further adding of surfactant enhanced the nucleate boiling regime heat flux by up to 300 percent. But, in the open literature, the information on the effect of dissolved surfactant in case of air atomized spray is not available. Therefore, further research is required in this regard. In open literature, the reported information [14] reveals that increasing the sub cooling delayed the onset of boiling but declined the slope of the nucleate boiling regime of the spray boiling curve. The increment in critical heat flux was relatively minor at low sub cooling and more significant at high sub cooling. The critical heat flux was enhanced by about 100 % when sub cooling was increased from 22 to 70 °C. but all the discussed information was provided for only at low substrate temperature. Refiners et. al [15] studied heat transfer during cooling in continue casting by water spray at various water temperatures. They noticed that heat transfer coefficient showed an increasing trend with increasing degree of sub cooling and also increasing spray mass flux. The work carried was on spray cooling with salt. The experiments were performed on a copper surface which was heated to a temperature of 240 °C [16]. Different types of salt were also considered in this study and their implication on surface heat flux is also studied. They found that heat transfer rate in this case of dissolved salt of MgSO₄ increased both in nucleate and transition boiling. Among all types of salt considered, MgSO₄ produced the largest increase in heat transfer rate. The flux showed an increasing trend with increasing salt concentration of 0.2 M and thereafter depicted a declining trend.

Based on the literature survey,

The main features of the present studies are:

- a) To see the effect of nozzle height and water flow rate on heat removal rate of spray cooling
- b) To know the effect of sea water concentration on heat transfer rate of spray cooling
- c) To study the effect of salt and surfactant mixed water on spray cooling
- d) Comparative study among all the processes

The main thesis has been presented in 4 chapters. Chapter 1 deals with the introduction and literature review. Chapter 2 focuses on the different characterization of spray, solution and material properties. It also includes a detailed description of experimental setup. Results and discussions are included in the chapter 3. And lastly, conclusions, future works and references have been presented in chapter 4.

Chapter 2

Experimental setup and characterization

2.1 Experimental setup and procedure

The experimental setup consists of three units. i.e. heating unit, cooling unit and imaging unit. The heating unit comprises of a muffle furnace which can heat the plate up to 1000 °C. Three sub surface thermocouples are introduced in the plate to measure the temperatures at different locations. Thermocouples are kept parallel to the impinging surface to eliminate the error occurred due to the thermocouple hole diameter. Furthermore, the thermocouples are connected to a data acquisition card for the recording of time-temperature histories during the cooling process. The heating element inside the furnace is Silicon carbide. The cooling unit consist of pump, water tank, nozzle, flow meters and pressure gauges. The water tank is connected to a centrifugal pump which supply the water to the rotameter through the solenoid valve. The rotameter is connected with a spray nozzle (LECHLER 490.804.1Y.CE).

A steel plate (AISI 304) having dimensions (100mm×100mm×6mm) is heated to a temperature of 1000°C in furnace. Three sub surface (K-type) thermocouples T/C1, T/C2 and T/C3 having position (20,3), (50,3) and (70,3) were used to measure the temperature during experiments.

After reaching the desired temperature (1000 °C) in the muffle furnace, the steel plate is taken out from the furnace and it is kept on the cooling pad. For spray, the water flow rate is set and pump and data logging system are also switched on for the measurement of temperature and supply of water respectively. The complete experimental set-up is given in Fig. 2.1. Initially the hot steel plate on the cooling pad is covered. When the spray reaches its usual state, it is allowed to impinge on the hot surface.

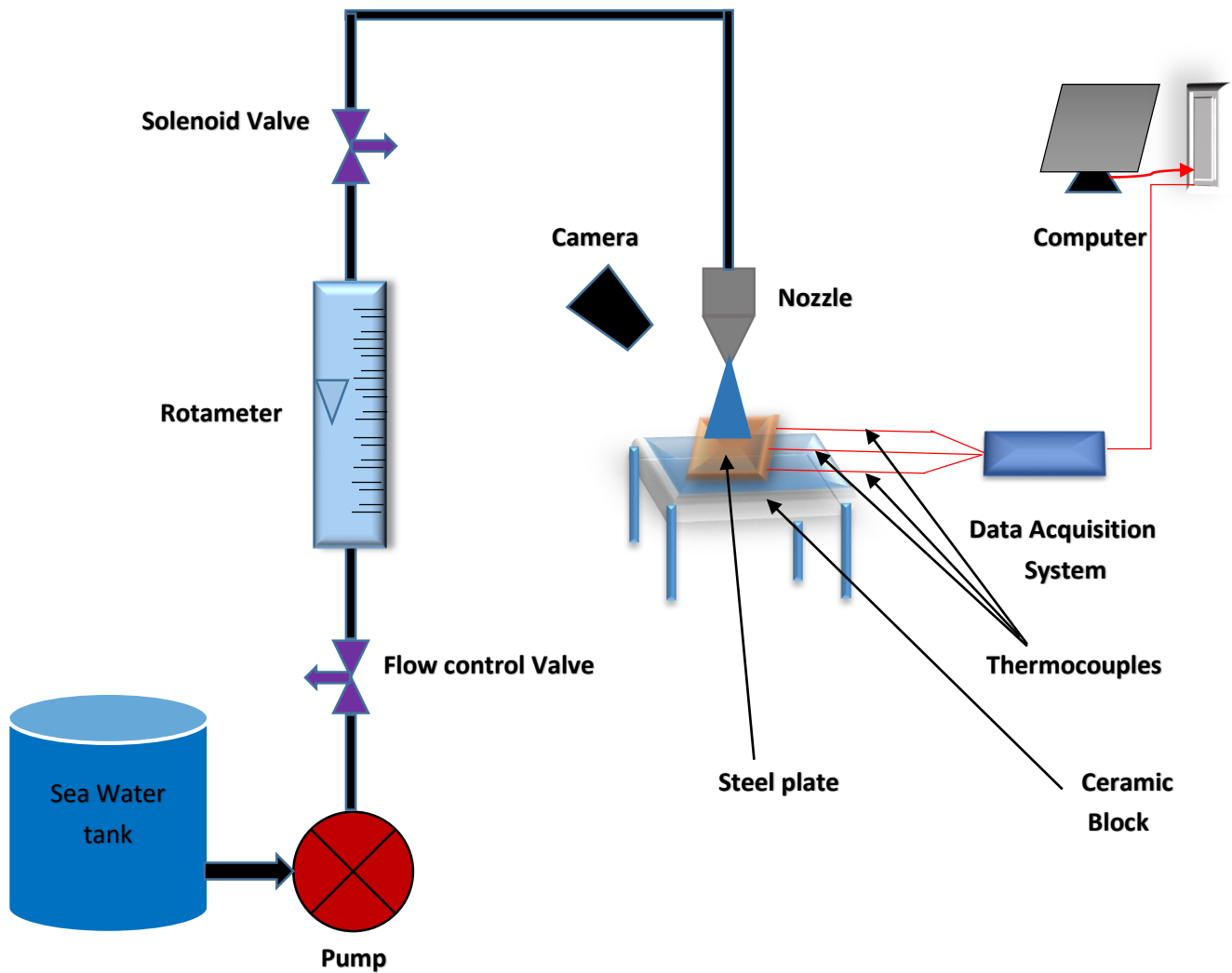


Fig. 2.1: Schematic diagram of the experimental setup

2.2 Calculation of surface heat flux and surface temperature by “INTEMP”

In the current work, inverse heat conduction method is used to calculate the heat flux and surface temperatures of surface by knowing the temperature on a known boundary developed by Trujillo and Busby (2003). It estimates the inaccessible surface boundary conditions using the accessible interior time-temperature histories. The input data to INTEMP program containing of a geometrical field, material conditions and the time-temperature histories measured by data

acquisition system (DAS). The procedure in calculating inverse heat conduction problems are as follows.

- 1) Initially, the software considers the heat flux as known initial condition, and estimates all the nodal temperature by using Crank-Nicolson method.
- 2) After that, the considered surface heat fluxes are calculated by a nonlinear optimization like least square method to decrease the error between the measured temperatures and the estimated nodal temperatures at the similar location.
- 3) When the error reaches minimum and heat flux reaches the optimum value, it predicts the exact temperature at each nodal point.
- 4) The technique converges when the minimum error is less than 0.02°C , unless it goes for the prediction of new surface heat flux and repeats until it reaches a least error.

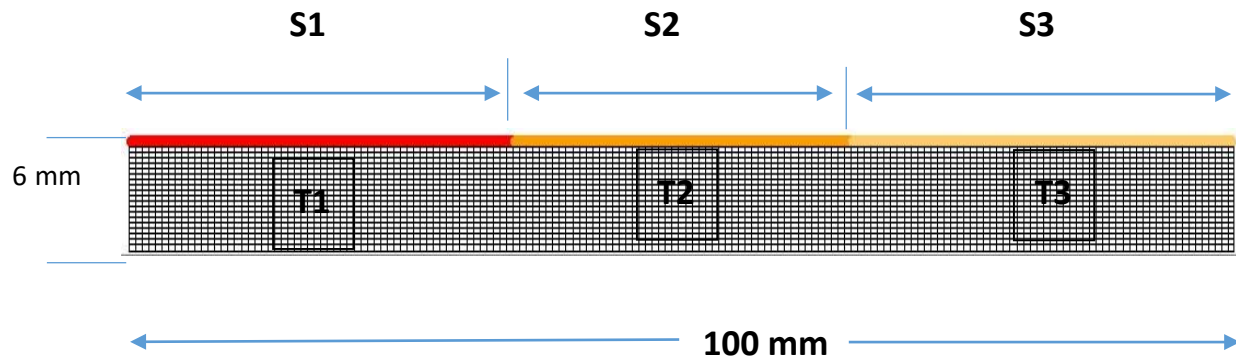


Fig. 2.2: Computational domain of the steel plate

The top non-adiabatic surface is distributed into three heat flux zones. The first zone is extending from $x = 0$ to 35mm (S1) and the second zone corresponds to $x = 35$ to 65mm (S2) whereas the third zone is from $x = 65$ to 100mm (S3).

2.3 Spray Characterization

Different properties of the droplet like impingement density, droplet velocity and droplet diameter which influence the heat transfer rate depend upon the water flow rates and each of them are described below.

2.3.1 Impingement density

The spray impingement densities measurement was carried out using a fabricated Patternator. The Patternator comprises of an array of glass tubes (5 mm diameter and 1 mm thick) as shown in Fig. 3. Water is collected in some interval of time (Δt) in each tube and the impingement densities are calculated by the following formula:

$$\dot{m}_s = \frac{4 M_w}{\pi d_t^2 \Delta t} \quad (1)$$

where \dot{m}_s = impingement density ($\text{kg}/\text{m}^2 \text{ s}$)

M_w = water flow rate (kg/s)

d_t = diameter of the tube (m)

Δt = time interval (s)



Fig. 2.3: Photograph of the Patternator (a) top view (b) side view

It can be seen from the Fig. 2.4 that with increasing water flow rate the local spray impingement density at any location shows an increasing trend.

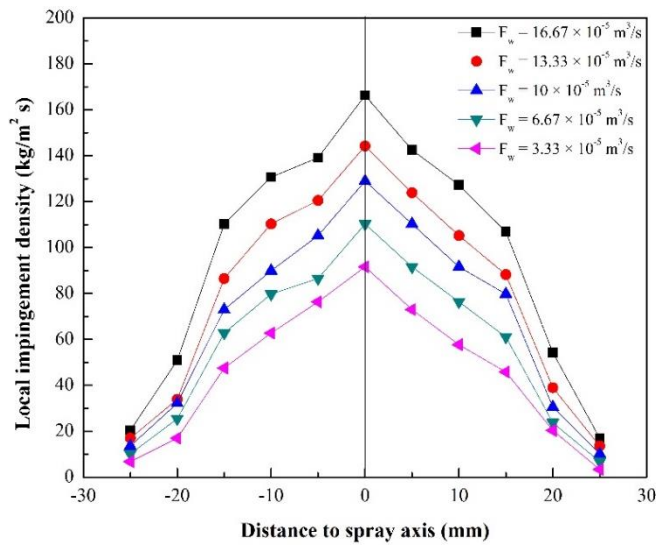


Fig. 2.4: Variation of local impingement density with varying water flow rate

2.3.2 Droplet velocity

The variation of droplet velocity with water flow rate is shown in Fig. 2.5. These data were supplied by the manufacturer. It is shown that with increasing water flow rate from 3.33×10^{-5} to $16.67 \times 10^{-5} \text{ m}^3/\text{s}$, the droplet velocity changes from 2 to 7.8 m/s.

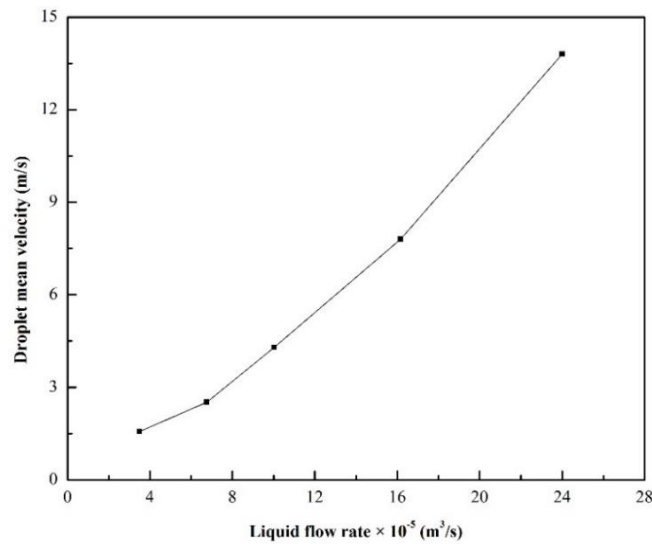


Fig. 2.5: Variation of droplet mean velocity with liquid flow rate

2.3.3 Droplet diameter

The variation of water flow rate with droplet diameter is shown in Fig. 2.6. Here, it can be seen that with increasing water flow rate droplet diameter shows an increasing trend. The spray experiment is conducted at different water flow rates. At each condition, the process is a steady state and moreover the discharge area is constant for all the cases. Hence, from the equation of continuity it can be said that an increasing flow rate mass flux increases and in turn droplet diameter. Maximum droplet diameter of 325.6 μm has been calculated at a water flow rate of $16.67 \times 10^{-5} \text{ m}^3/\text{s}$.

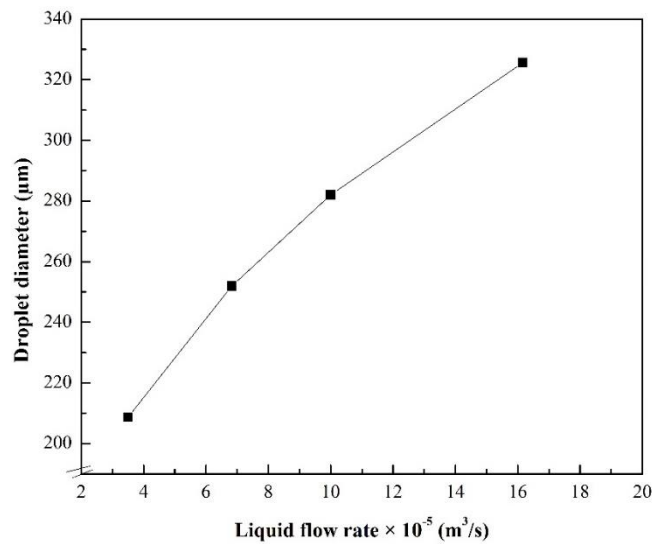


Fig. 2.6: Variation of droplet diameter with liquid flow rate

2.3.4 Spray pressure

The variation of spray pressure and water flow rate is shown in Fig. 2.7. This happens because of increasing water flow rate the pressure energy increases within the nozzle. When the spray area is exposed to open atmosphere, suddenly area increases and as a result the pressure energy converts into the kinetic energy.

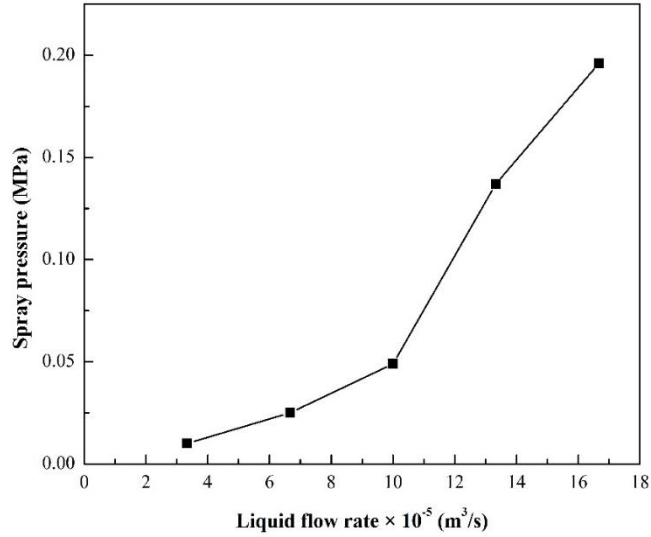


Fig. 2.7: Variation of spray pressure with liquid flow rate

2.4 Material Characterization

The material properties play an important role, which require in the calculation of surface tension and temperature. In the current case, the material on which quenching experiments were conducted, its compositions were measured with the help of optical emission spectrophotometer (OES). The obtained composition (Table 2.1) is then compared with the standard composition. The comparison confirms AISI-304 standard. The material properties at different temperature of AISI-304 standard steel plates are available in the open literature. Hence, from the literature the material properties have been taken. The Table 2.2 shows the material properties of AISI-304 standard steel plate.

Table 2.1: Composition the material used in the experimentations (% weight)

C	Cr	Fe	Mn	Ni	P	S	Si
0.08	18.20	66.74	1.18	8.5	0.043	0.03	0.95

Table 2.2: Material properties (at 25 °C)

Density (kg/m ³)	8000
Thermal conductivity (W/m °C)	16.2
Specific heat capacity (kJ/kg °C)	0.5

2.5 Solution Characterization

In case of fast quenching process, the coolant properties decide the final heat transfer rate and the heat transfer mechanism. The coolant properties which are related to the spray cooling are heat transfer area, specific heat capacity, thermal conductivity and mass diffusivity.

2.5.1 Contact angle

The heat transfer area in case of dropwise evaporation process is directly related to the contact area and contact angle of the coolant with the hot substrate. Therefore, in the current work droplet contact angle were measured at different salt concentration and different sea water concentration which are shown in Fig. 2.8 and 2.9 respectively. The contact angle of NaCl added water increases with increasing salt concentration. This is due to the dissolution of NaCl in the bulk of water instead of the surface. In addition to the above similar trend line is observed for the case of sea water which shows an increasing trend of NaCl with the decreasing dilution.

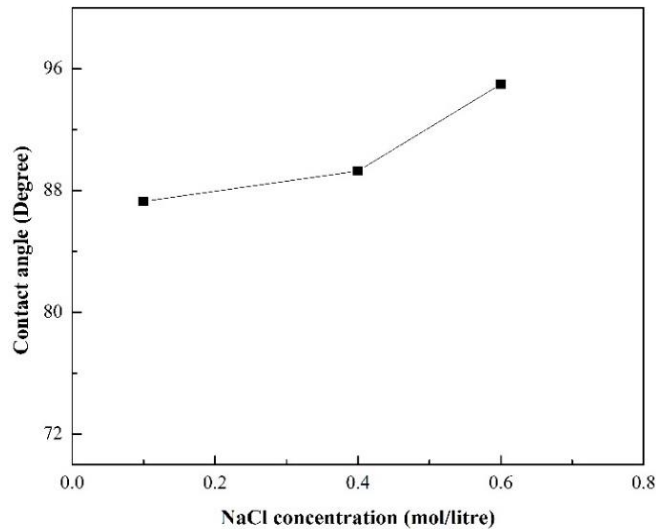


Fig. 2.8: Variation of contact angle with salt concentration

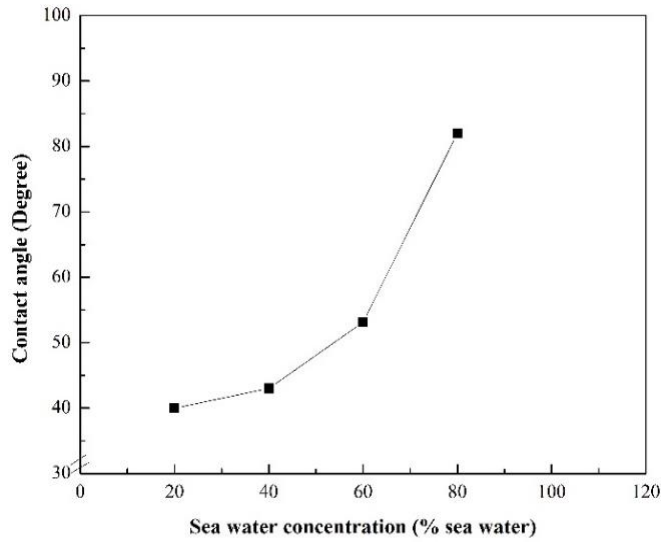


Fig.2.9: Variation of contact angle with sea water concentration

2.5.2 Specific heat capacity, thermal conductivity and diffusivity

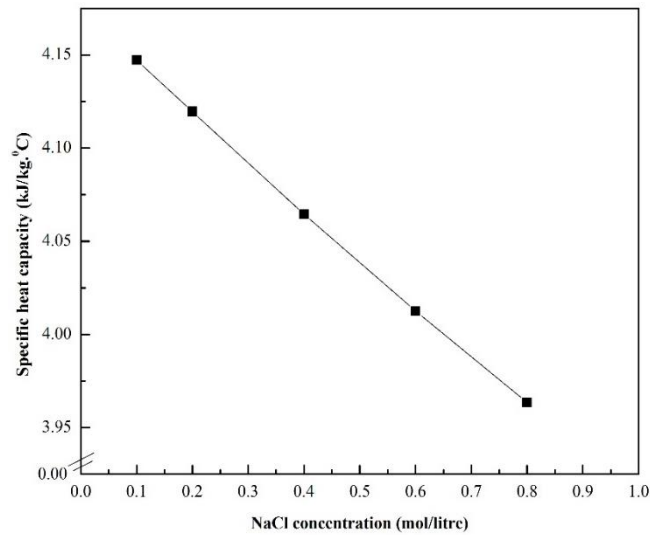


Fig. 2.10: Variation of specific heat capacity with salt concentration

In case of film boiling or transition boiling, the heat transfer coefficient is a function of specific heat capacity and thermal conductivity. The variation of these values with respect to salt concentration are shown in Fig. 2.10 and 2.11 respectively. The specific heat capacity value decreases with increasing salt concentration and this is a favorable condition for fast quenching process. However, the thermal conductivity depicts a decreasing trend with increasing salt concentration. The evaporation of single salt added water droplet reveals that salt deposits on the

hot surface during the evaporation process. This rate of deposition is mainly controlled by diffusivity value. In the present work, the variation of diffusivity with the salt concentration is shown in Fig. 2.12.

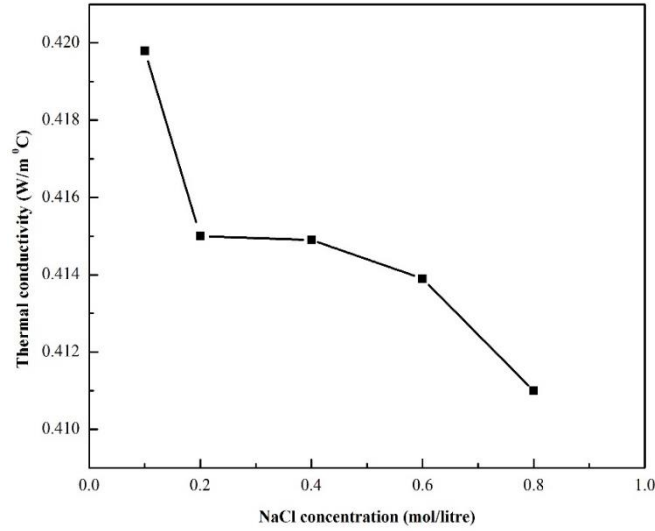


Fig. 2.11: Variation of thermal conductivity with salt concentration

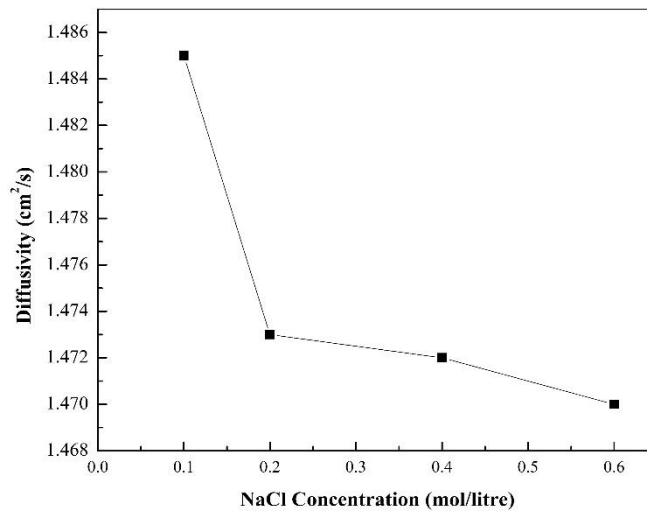


Fig. 2.12: Variation of diffusivity with salt concentration

Chapter 3

Results and Discussion

3.1 Spray cooling by pure water

In case of spray cooling by pure water, the droplet momentum plays an important role and this is related to the nozzle height and water flow rate. Hence, initially the effect of aforesaid variables is studied.

3.1.1 Effect of nozzle height

For the study of the effect of nozzle height, different experiments were conducted at different nozzle heights and at various water flow rates. The effect of nozzle height at aforesaid maintained water flow rate is shown in below figure. For all the nozzle heights, the maximum heat transfer rate is obtained at water flow rate of $16.67 \times 10^{-5} \text{ m}^3/\text{s}$. Fig. 3.1 indicates the variation of surface heat flux with cooling time. The plot clearly depicts domination of heat for the height of 20 mm.

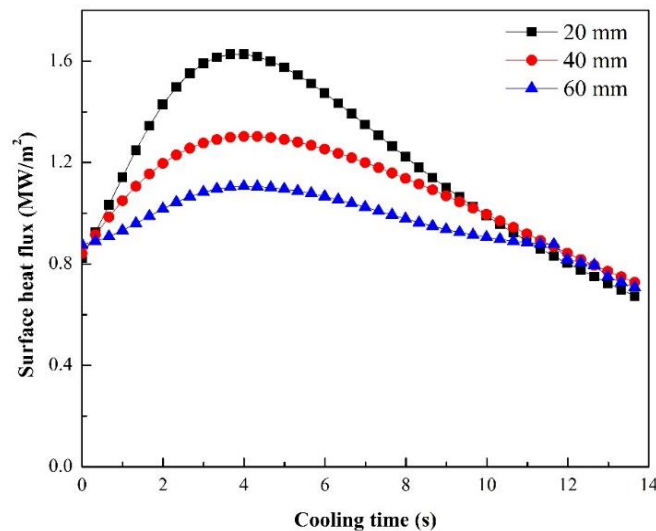


Fig. 3.1: Variation of surface heat flux with time

With the decreasing nozzle height, the droplet momentum increases and spray area decreases. When both the phenomena are considered together, it is found that the average surface heat flux increases up to nozzle height 40 mm and thereafter declines. To understand the aforesaid phenomena more clearly, the average heat flux and the spray area have been calculated at different

nozzle heights and these are presented in Table 3.1. It shows that the spray area increases with increasing nozzle height whereas the average heat flux increases up to a nozzle height of 40 mm and then decreases. The maximum effect of combined effect of spray area and droplet momentum on cooling is noticed at nozzle height of 40 mm and hence the second the condition of Table 3.1 is selected.

Table 3.1: Variation nozzle height with spray area and average surface heat flux

Nozzle height (mm)	Spray area $\times 10^{-4}$ (m ²)	Average surface heat flux (MW/m ²)
20	8.709	0.80930
40	28.27	0.88872
60	50.24	0.66277

3.1.2 Effect of water flow rate

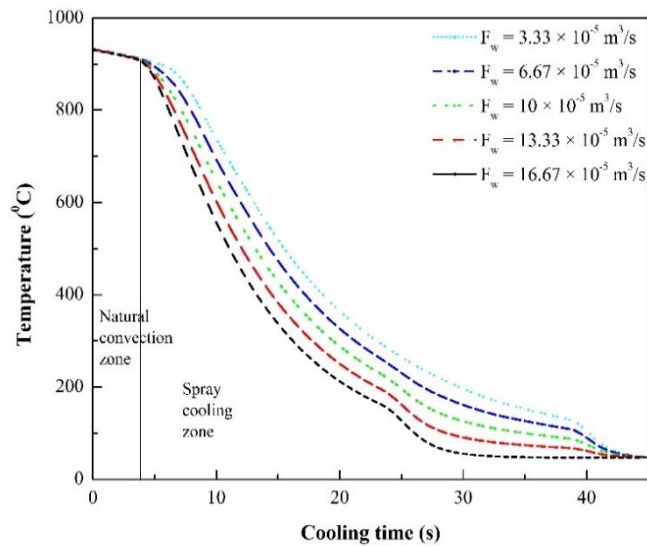


Fig. 3.2: Variation of sub surface temperature with time

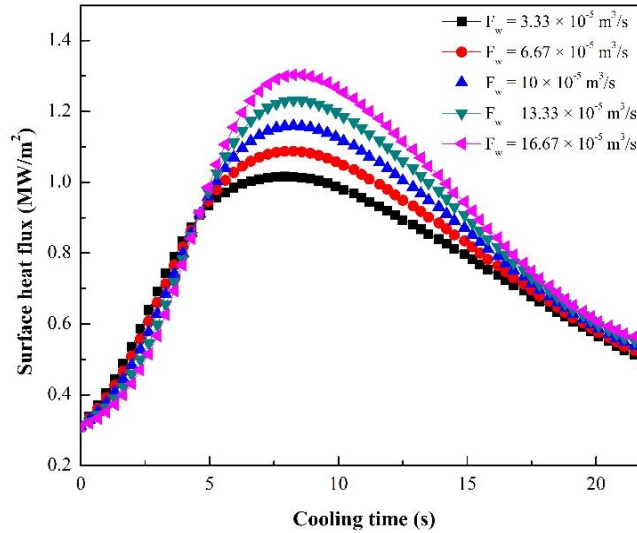


Fig. 3.3: Variation of surface heat flux with time

As per the experimental design, five number of experiments were conducted to find out the optimum flow rate at a constant nozzle height of 40 mm. The temperature-time histories for each experiments were recorded by using DAQ system.

The temperature-time histories measured at different flow rates by the thermocouple (T/C2) at the central position (50, 3) are shown in Fig. 3.2. Before the experimentation, all the thermocouples indicate the equal temperature which ensure the suitable thermal soaking of the steel plate inside the furnace. Initial 4.5 s of cooling is due to natural convection which occurs due to bringing the steel plate from the furnace to the resting pad. The cooling zone after 4.5 s corresponds to spray cooling. The plot (Fig.3.2) depicts that by increasing water flow rate cooling time decreases. This is described by the fact that higher mas flux leads to higher cooling rates.

Variation of surface heat flux with time at different water flow rate is presented in Fig. 3.3. Each curves in Fig. 3.3 is showing the same trend. The said figure shows an increasing trend of surface heat flux up to 9 s. At this point, the highest value of surface heat flux is achieved. Therefore, it follows a constant decreasing trend. The increasing trend is observed due to the initial onset of transition boiling regime whereas the decreasing trend corresponds to the nucleate boiling regime (Fig. 3.3). Fig. 3.4 depicts the variation of surface heat flux with surface temperature which is also known as boiling curve. All the curves in the Fig. 3.4 are showing same trend i.e. increasing up to a temperature of 500⁰ C and decreases thereafter. It is depicted that the boiling curves first follow transition boiling regime and then nucleate boiling regime which correspond to significant

amount of heat loss. It should be noted that on increasing water flow rate from $3.3 \times 10^{-5} \text{ m}^3/\text{s}$ to of $16.67 \times 10^{-5} \text{ m}^3/\text{s}$, the heat flux increases with increasing surface temperature. The maximum heat flux was achieved for water flow rate $16.67 \times 10^{-5} \text{ m}^3/\text{s}$ at a surface temperature of 500°C .

From Fig. 3.3, it is depicted that minimum surface heat flux removal rate is observed at a water flow rate of $3.3 \times 10^{-5} \text{ m}^3/\text{s}$. By increasing water flow rate, surface heat flux rises and it gives a maximum value of $1.29 \text{ MW}/\text{m}^2$ at a water flow rate of $16.67 \times 10^{-5} \text{ m}^3/\text{s}$. The aforesaid cooling enhancement is described with help of a schematic diagram (Fig. 3.5). In the case of low momentum (Fig. 3.5a), the water droplet cannot penetrate through the vapour layer and water layer as a result the heat transfer occurs by convection. But in Fig. 3.5b, due to high momentum, the water droplet penetrates the vapor film and reaches the hot surface, so the heat transfer in the current case occurs due to conduction. As the heat transfer rate in case of conductive mode is higher than convective mode, the heat transfer rate increases with increase in water flow rate which is directly proportional to droplet momentum (Fig. 2.5) So, in the current case the optimum value is considered is $16.67 \times 10^{-5} \text{ m}^3/\text{s}$.

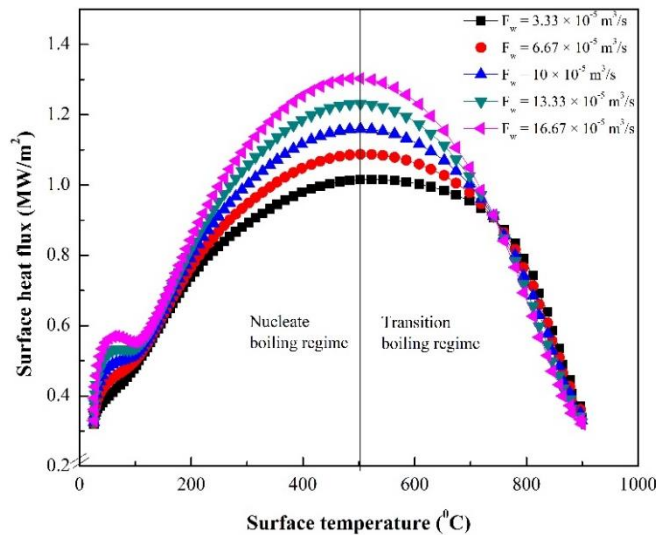


Fig. 3.4: Variation of surface heat flux with surface temperature

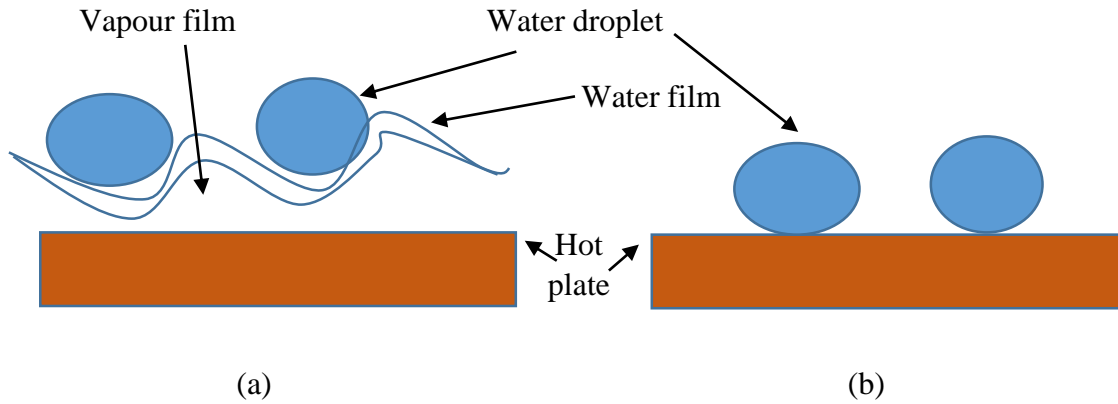


Fig. 3.5: Schematic diagram in case of (a) low momentum droplet (b) high momentum droplet

The variation of average heat flux and average cooling rate with different flow rates are shown in Fig. 3.6 and Fig. 3.7 respectively. The average heat flux and average cooling rates data have been calculated in the temperature range between 900° - 600° C. From the Fig. 3.6, it is shown that by increasing water flow rate the average surface heat flux increases and similar trend line the cooling rate also depicts.

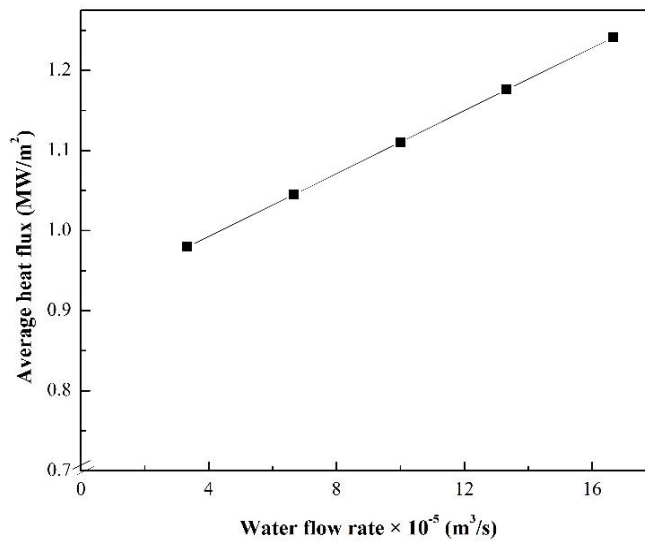


Fig. 3.6: Variation of average heat flux with different water flow rates

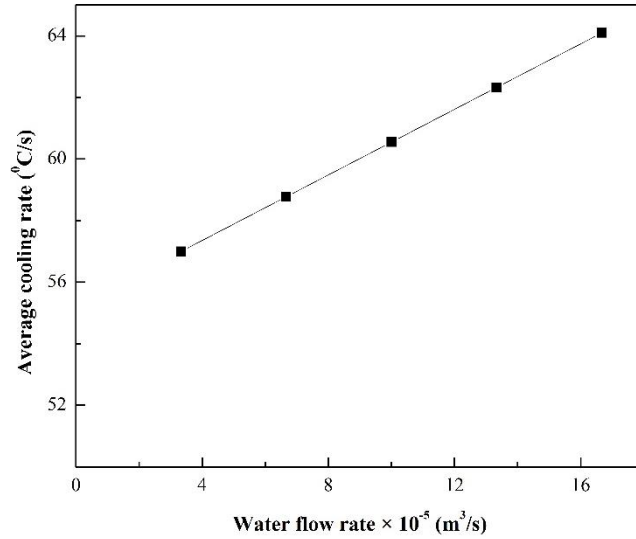


Fig. 3.7: Variation of average cooling with different water flow rates

The rate of propagation of forced convection cooling area (Fig. 3.8) in the hot plate decides the final cooling rate. To verify the cooling enhancement, the forced convection cooling area with different flow rates and also at different time were calculated. For this purpose, a number of photographs were taken during experimentation which is shown in Fig. 3.8. The dark portion is the forced convection cooling zone. At $t = 10.8$ s, the dark zone diameter covers the hot plate partially for flow rate $3.3 \times 10^{-5} m^3/s$, whereas at the same time for the flow rate of $16.67 \times 10^{-5} m^3/s$ the plate is totally covered by the dark zone diameter. Hence, it is concluded that the heat removal rate is enhance in case of higher flow rates.































Water flow rate $\times 10^{-5}$ (m ³ /s) Time (s)	3.33	6.67	10	13.33	16.67
0.1					
2.7					
4.9					
10.8					
15.7					
22.7					

Fig. 3.8: Visual observation of experiments conducted at different water flow rates

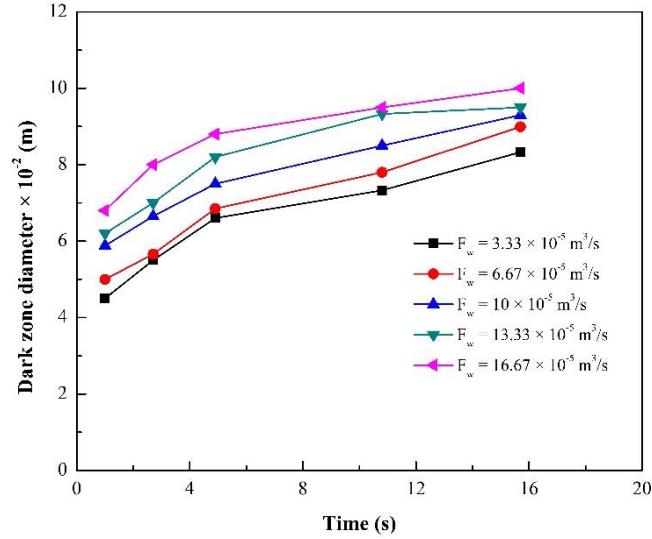


Fig. 3.9: Variation of dark zone diameter with time

The calculation of dark zone diameter or forced convection cooling zone with time (Fig. 3.9) confirms the aforesaid conclusion.

3.2 Salt added spray cooling

To see the effect of dissolved salt in droplet evaporation, experiments were conducted at different salt concentration. The followings are the results from the said study.

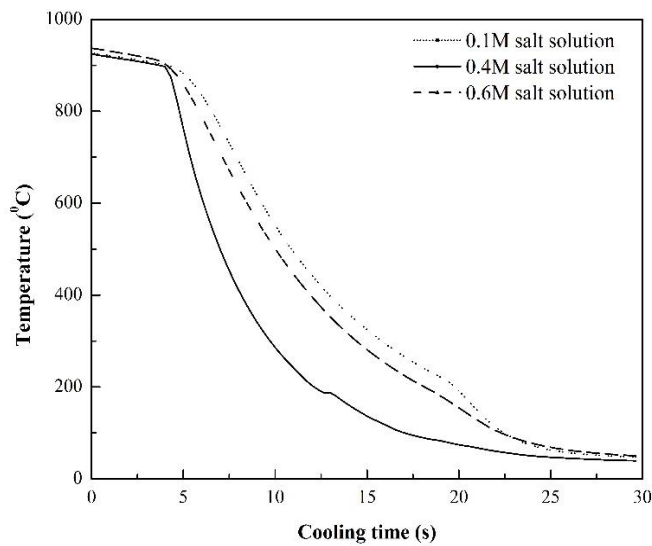


Fig. 3.10: Variation of sub surface temperature with time

3.2.1 Effect of salt added water

The variation of temperature with time and surface heat flux with time are shown in Fig 3.10 and 3.11, respectively. The effect of temperature with time at different concentrations of NaCl are depicted in Fig. 3.10. All the experiments were conducted with different salt solutions at a water flow rate of $16.67 \times 10^{-5} \text{ m}^3/\text{s}$ and a constant nozzle height of 40 mm. It is noted that all the curves in the Fig. 3.10 shows same trend and up to initial 5 s, which corresponds to the natural convection. After this time, the heat loss increases rapidly due to increase in time because of spray cooling. The cooling time for 0.4 M salt solution to reach $900^0\text{-}600^0\text{C}$ is 7 s where as it takes 9.5 s and 10 s for 0.6 M and 0.1 M salt solution respectively.

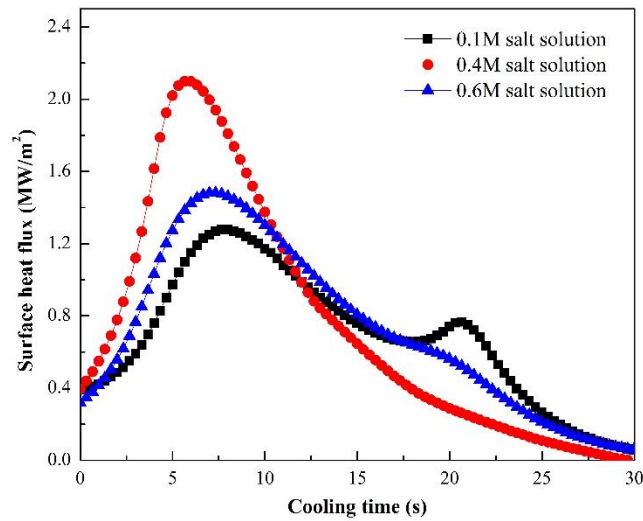


Fig. 3.11: Variation of surface heat flux with time

Variation of surface heat flux with time is depicted in Fig. 3.11. The heat flux initially shows an increasing trend and then a decreasing trend with cooling time. In the nucleate boiling regime, i.e. from 10 s to 15 s, the cooling enhancement is due to the promotion of nucleate boiling and prevention of bubble coalescence.

For the better understanding, in case of spray cooling, the salt deposition phenomena are described with the help of a schematic diagram (Fig.3.12). It describes that how salt gets deposited on the surface. When the salt added water droplet touches the hot plate stage 1. The local temperature of side (1) of stage 1 increases. As a result, evaporation starts from side (1), and this is shown in the stage 2. Due to this process the local salt concentration of salt in side (1) increases and concentration gradient between side (1) and (2) develops.

Because the residence time of the droplet is lower than the diffusing time of salt from side (1) to side (2). As a result, some amount of the salt deposits on the evaporating location which is shown in stage 3 of Fig. 3.12.

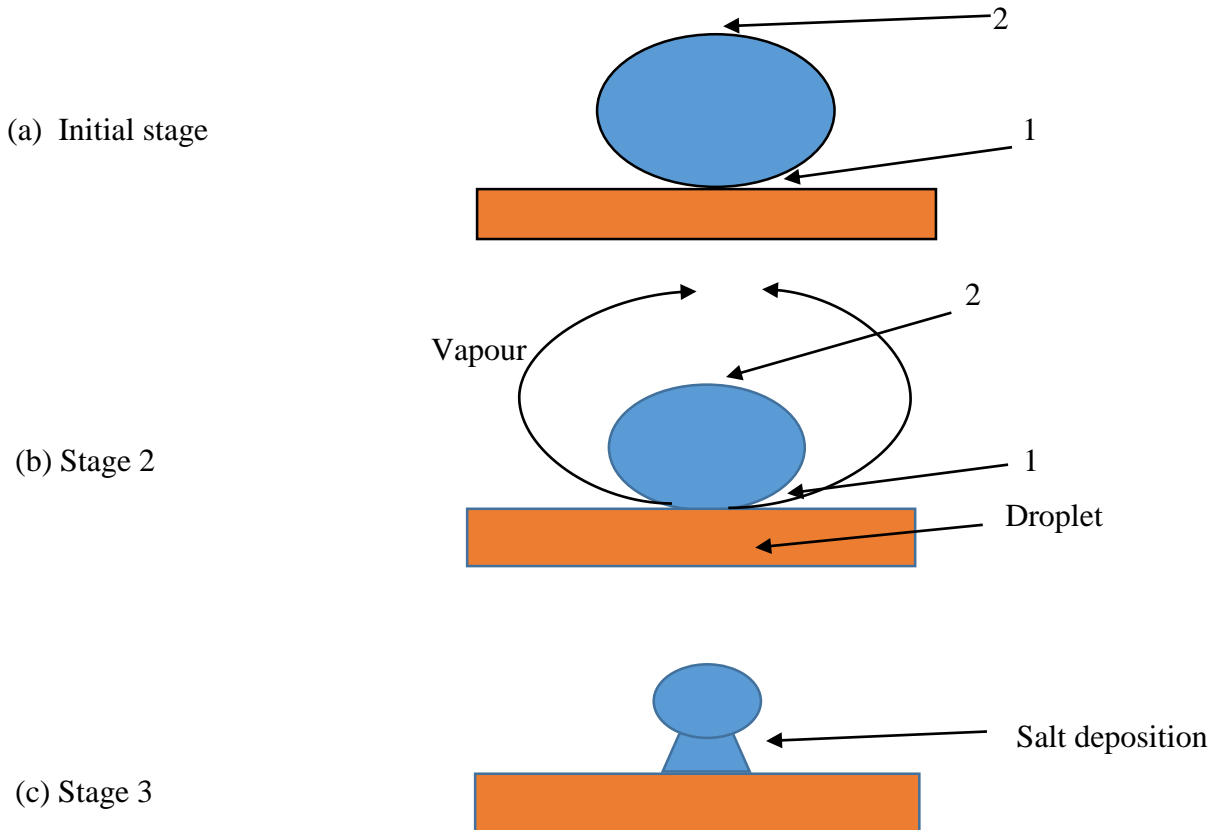


Fig. 3.12: Schematic diagram showing the mechanism of salt deposition

Due to this salt deposition phenomena, the incoming droplets impinges on the salt. As a result, the heat transfer proceeds from the hot surface to the water droplet by conduction mode through the deposited salt. This change in heat transfer mechanism from convection mode (film boiling case) to conductive mode (salt deposition case) the heat removal rate increases and this is shown in Fig. 3.11.

Fig. 3.11 also shows that the heat removal rate increases up to salt concentration of 0.4 M and thereafter decreases. Up to the salt concentration 0.4 M, salt deposition phenomenon dominates over film boiling phenomenon. However, beyond the aforesaid concentration high amount of deposition on the hot plate has been noticed. Although this deposition reduces the film

boiling affect, however the conductive heat transfer rate decreases with increment of salt deposition. With increasing salt deposition, the net thermal conductivity ($k_{\text{salt}} + k_{\text{plate}}$) becomes lower than the minimum salt deposition case. This is shown in a schematic diagram (Fig. 3.13).

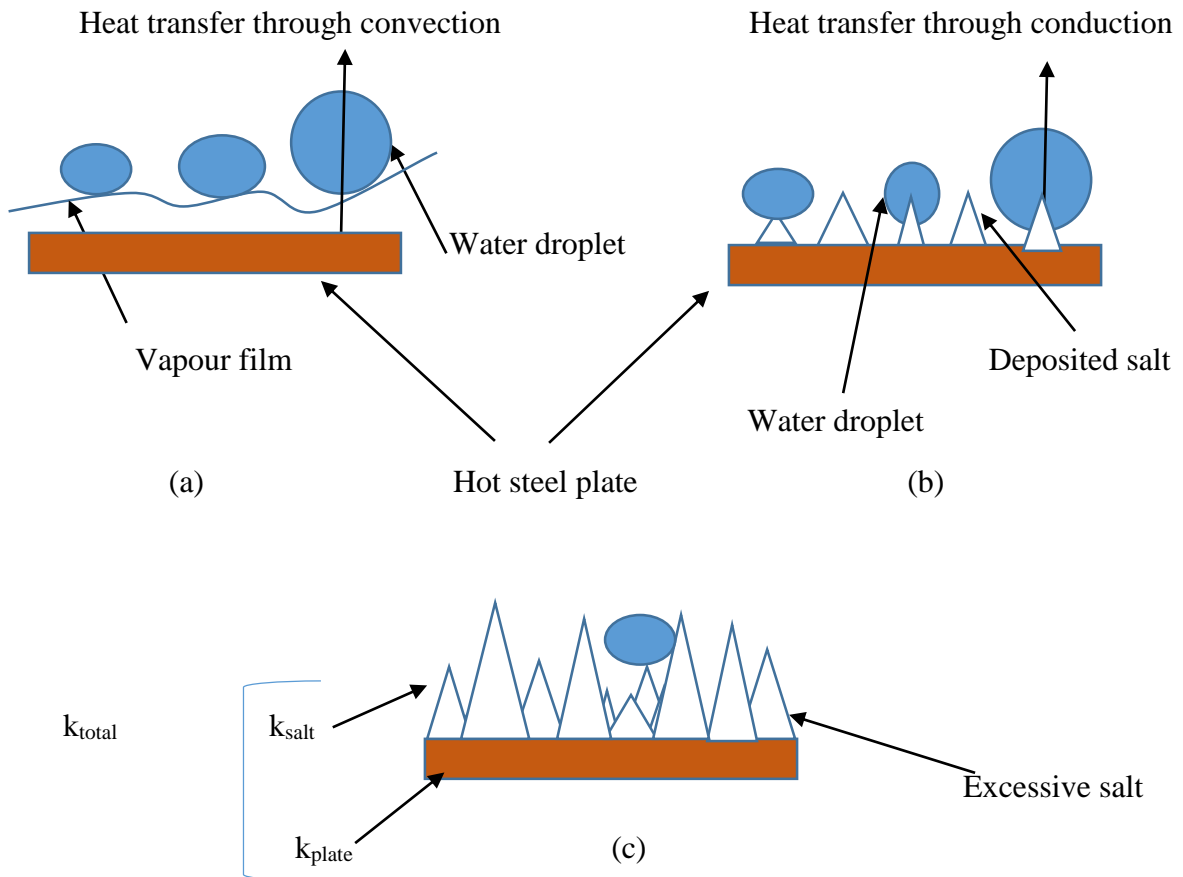


Fig. 3.13: Schematic diagram of spray evaporative cooling by (a) pure water (b) 0.4M salt solution (c) 0.6M salt solution

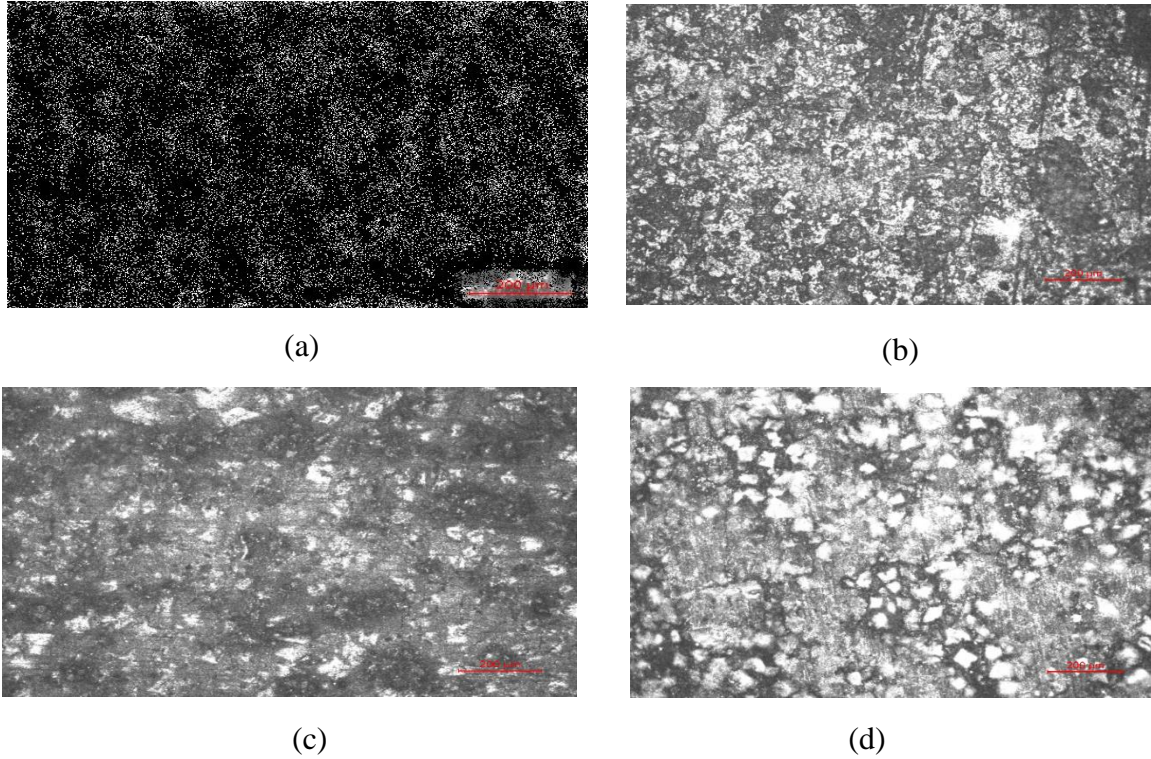


Fig. 3.14: Microscopic images of steel plate (a) and after cooling with (b) 0.1M salt solution (c) 0.4M salt solution (d) 0.6M salt solution

Table 3.2: Amount of salt deposited on the steel plate

Feed Concentration	Measured Concentration	Amount of salt deposited on the surface of the plate (No. of moles)
0.4 M NaCl	0.010 M	0.0002
0.6 M NaCl	0.015 M	0.0003

After salt added water spray cooling, for the verification of salt deposition, surface images were taken by using a microscope at very high magnification and these images (Fig 3.14) clearly depicts the salt deposition when these are compared with untreated substrate. This is due to the lowering of diffusivity values with the salt concentration. For more verification of the salt

deposition, after experimentation, the heat treated samples were washed with distilled water and the concentration of the above mentioned water examined. The obtained results were shown in Table 3.2. This table clearly indicates increment of salt deposition with the increment of salt concentration.

For better understanding of heat transfer technique of the boiling curve of salt added spray cooling is shown in Fig. 3.15. From the figure below, transition boiling regime falls in the temperature range of 900–700⁰C, and the surface heat flux touches the maximum value of 2.1 MW/m² at T = 700⁰C. Thereafter, the heat flux declines with drop in surface temperature, due to the boiling regime from transition shifts to nucleate boiling regime.

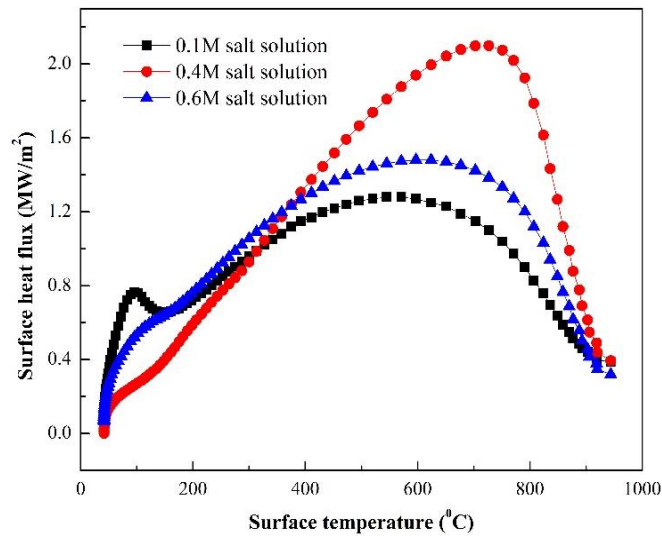


Fig. 3.15: Variation of Surface heat flux with surface temperature

The average heat flux and the average cooling rate have been calculated for the surface temperature falls from 900⁰ C to 600⁰ C. Fig. 3.16 depicts the variation of average heat flux with varying salt concentration. It is seen that by increasing salt concentration, the average heat flux increases up to a salt concentration of 0.4 M.

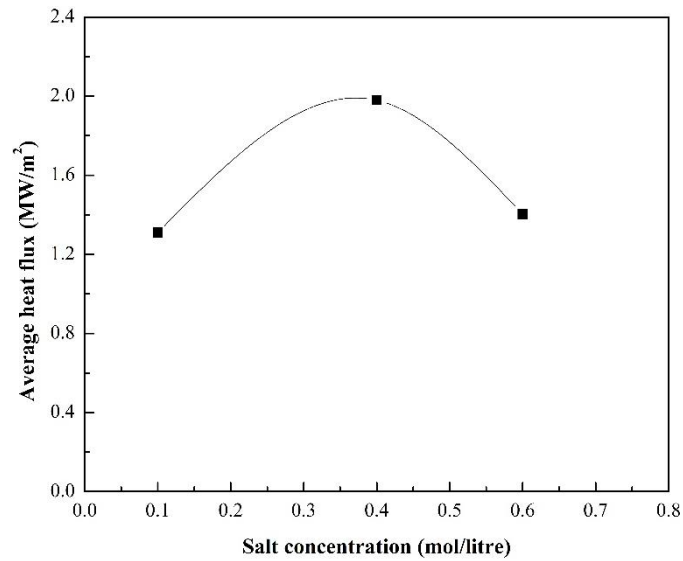


Fig. 3.16: Variation of average heat flux with salt concentration

The trend of average surface cooling rate with different NaCl concentration is given in Fig. 3.17. This figure depicts that cooling rate increases with increase in NaCl concentration and reaches a optimum value at 0.4 M salt concentration. Further, the cooling rate decreases with rise in salt concentration. A maximum 120 °C/s is achieved at a salt concentration of 0.4 M.

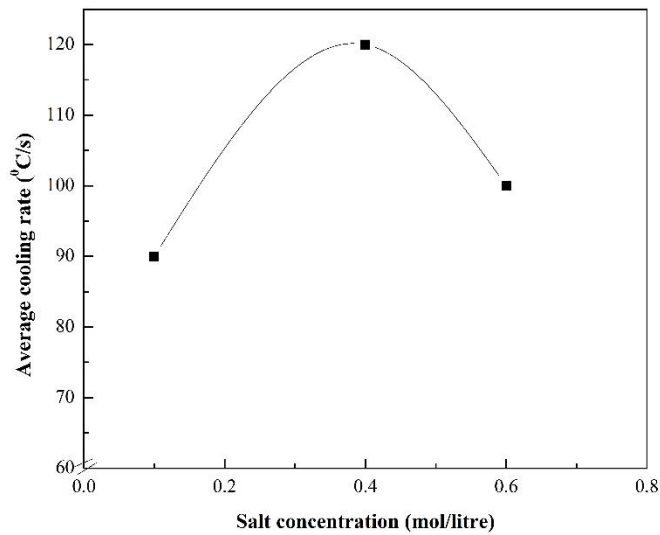


Fig. 3.17: Variation of average cooling rate with salt concentration


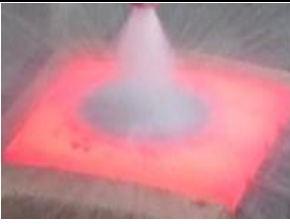
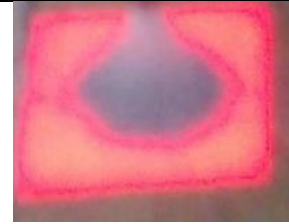









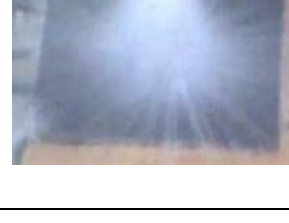
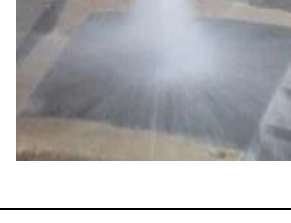
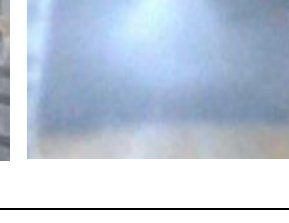
Salt solution (mol/litre)	0.1	0.4	0.6
Time (s)			
0.1			
3.1			
6.1			
10.1			
14.1			

Fig. 3.18: Visual analysis of the experiments conducted with different salt solution

For the verification of cooling enhancement, photographs (Fig. 3.18) were taken and the propagation of forced convective cooling zone or dark zone diameter have been calculated. The progress rate of forced convection cooling zone confirms the cooling enhancement.

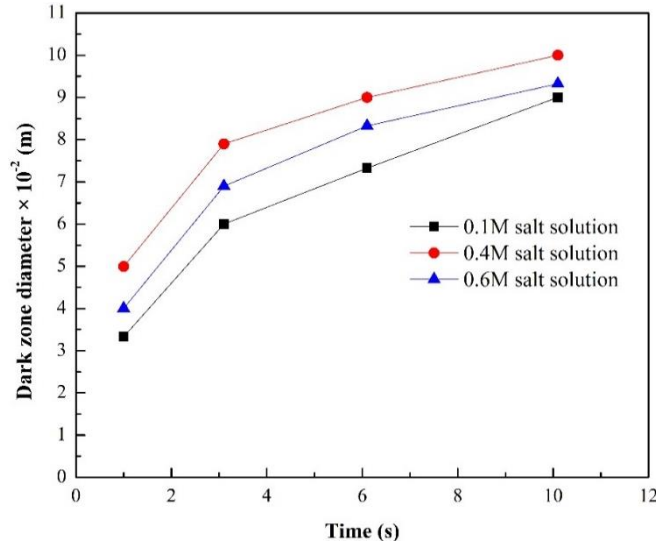


Fig. 3.19: Variation of dark zone diameter with time

For the calculations of dark zone diameter, a sequence of images taken during experiment. The Fig. 3.19 depicts the variation of dark zone or forced convection cooling zone diameter with time at various salt concentrations. The forced convection cooling zone diameter increases with increase in time to a salt concentration of 0.4M, and then declines. This is due to the excessive deposition of salt in case of high concentration as described in the Fig. 3.13(c).

3.3 Surfactant added spray cooling

3.3.1 Effect of surfactant added water

One of the important parameter that affects the heat transfer rate is heat transfer area. On increasing the heat transfer area, area for heat transfer will be more as a result, heat transfer rate increases. The heat transfer area can be increased by reducing the contact angle of the coolant droplets with the hot surface. This is achieved by addition of surfactant in coolants.

In the current work non-ionic surfactant polyoxyethelene (20) sorbitan monolaurate (Tween 20) having chemical formula $C_{18}H_{34}O_6(C_2H_4O)_{20}$ is used. The main advantage of Tween

20 is that less concentration of surfactant is required to lower the surface tension and also less foaming occurred. At optimum concentration (56 ppm) experiment was conducted.

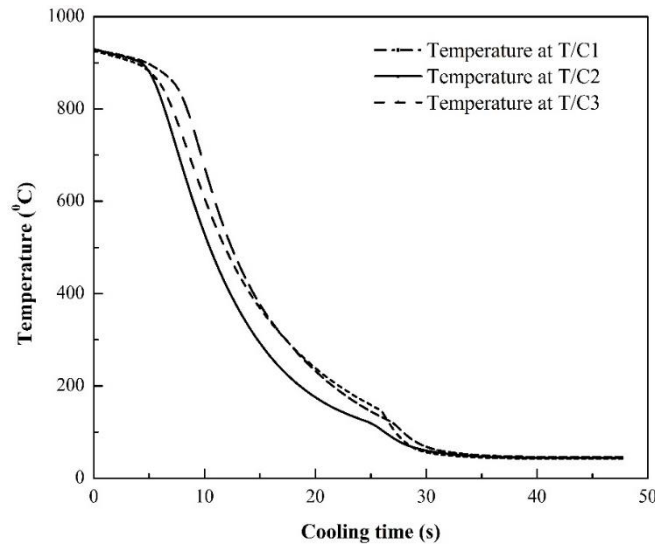


Fig. 3.20: Variation of temperature with time

Fig. 3.20 represents the variation of temperature with time. The experiment is carried out at a water flow rate of $16.67 \times 10^{-5} \text{ m}^3/\text{s}$ and 56 ppm as surfactant concentration. The time-temperature histories are recorded by DAS system is shown in Fig. 3.20. The temperature drops in case of thermocouple only T/C 2 is more fast as compared to other thermocouples. This is because only thermocouple T/C 2 is directly under spray area.

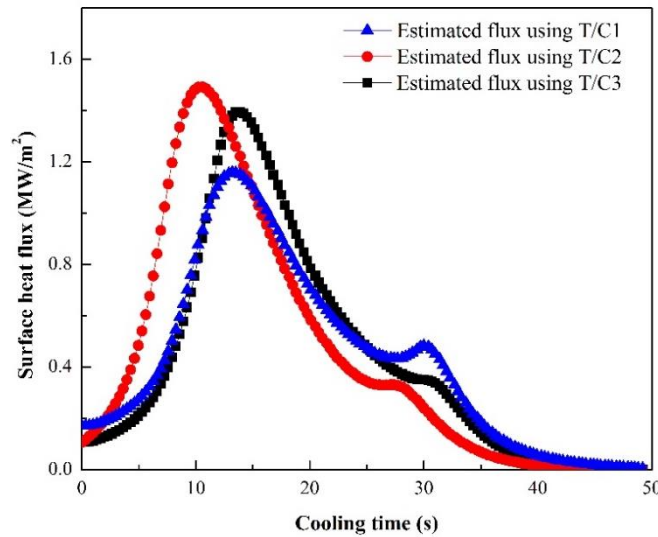


Fig. 3.21: Variation of surface heat flux with time

Fig. 3.21 shows the variation of surface heat flux with time. It is seen that all the curves are showing the same trend. The heat flux estimated using the thermocouple (T/C 2) shows the maximum critical heat flux among the three trends. The thermocouple T/C 2 is positioned under the surface heat flux zone S2 as shown in Fig 2.2. This heat flux zone is under direct impingement zone. Therefore, surface heat flux calculated are maximum in this zone.

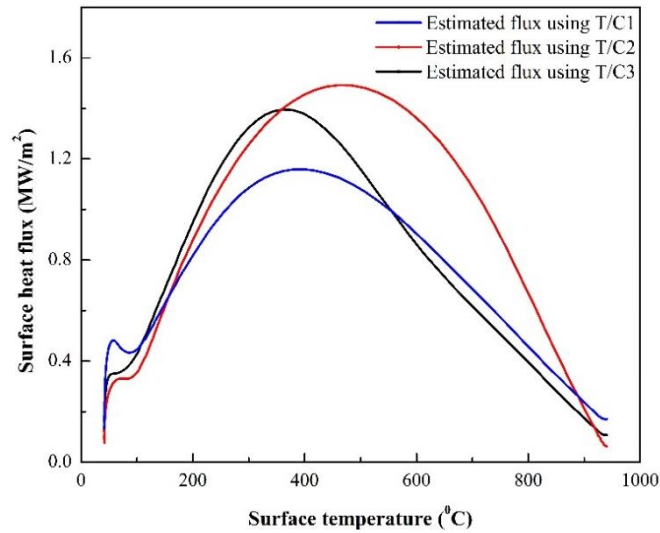


Fig. 3.22: Variation of surface heat flux with surface temperature

The effect of surface heat flux with surface temperature is shown in Fig. 3.22. The transition boiling region lies in the temperature range from 900°C to 600°C and beyond this range nucleate boiling occurs.

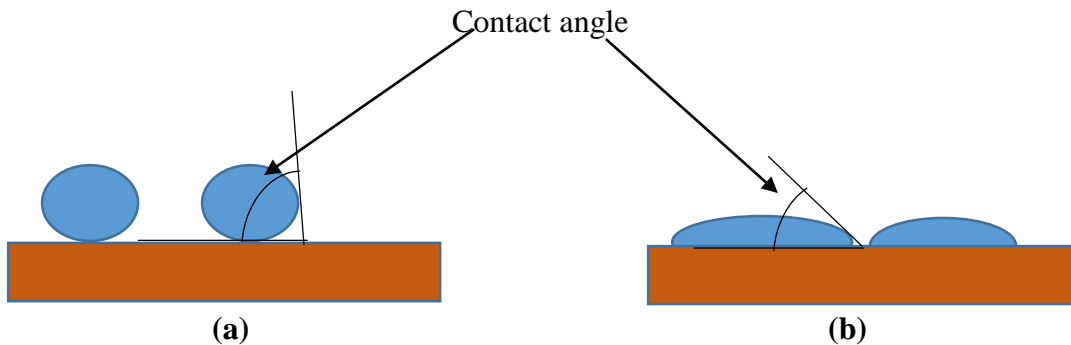


Fig. 3.23: Schematic diagram of spray cooling with (a) pure water (b) surfactant added water

The heat transfer mechanism associated with the surfactant added water is described by a schematic diagram shown in Fig. 3.23. Addition of surfactant with water, decreases the droplet contact angle with the solid surface which in turn increases contact heat transfer area. So, the heat transfer rate from the hot plate is faster in the current case than in the case of pure water (Fig. 3.23a).

3.4 Sea water added spray cooling

3.4.1 Effect of sea water on spray cooling

There are various properties that effects the heat transfer such as contact angle, thermal conductivity, surface tension, density, viscosity, salt deposition rate etc. From the said favorable properties for heat transfer, few properties are seen in case of sea water. As the sea water contains both the properties of salt and surfactant, in the current study sea water is used. The experiments were carried out by varying the sea water concentration by adding pure water with an optimum flow rate of $16.67 \times 10^{-5} \text{ m}^3/\text{s}$ and a nozzle height of 40 mm. The concentration was varied by adding a proportion of water with sea water. i.e. 60 % sea water concentration corresponds to 60 % sea water plus 40 % pure water.

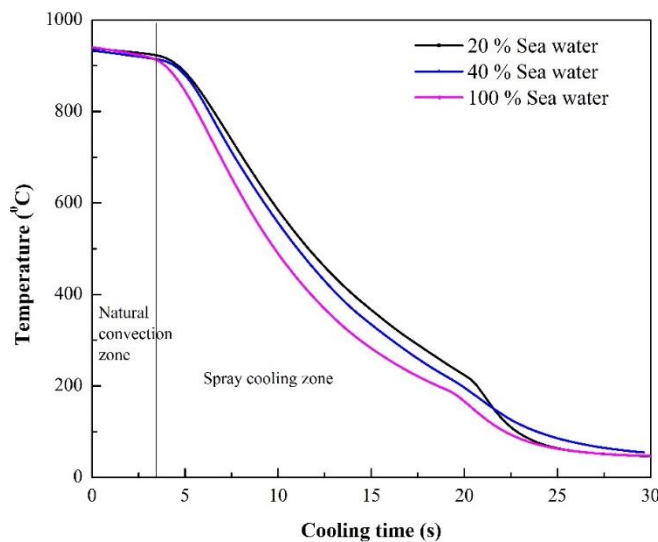


Fig. 3.24: Variation of temperature with time

The final set of experiments were conducted varying the sea water concentration by keeping the water flow rate $16.67 \times 10^{-5} \text{ m}^3/\text{s}$ and nozzle height 40 mm as constant. Fig. 3.24 shows the variation of sub surface temperature with respect to time. All the curves show the same trends.

The initial 3.5 s of cooling occurs due to natural convection and thereafter the curve shows a sharp temperature drop which corresponds to the spray cooling region. As seen from the above figure, by increasing sea water concentration, time taken to cool the hot plate decreases. Hence, the time required to reach 900⁰-600⁰C temperature drop for 100 % sea water is 7.5 s where as it is 10 s and 11 s for 60 % and 20 % sea water respectively.

The variation of surface heat flux with time is shown in Fig. 3.25. Initially all the curves depict an increasing trend, and thereafter declines. From the Fig. 3.25 it can be seen that a maximum critical heat flux of 1.5 MW/m² is achieved for 100 % sea water at 7.5 s and by decreasing sea water concentration the critical heat flux decreases. This is due to the fact that sea water contains properties of both salt and surfactant. Salt reduce the film boiling phenomena and in addition surfactant reduce the contact angle which enhance the heat transfer area. As a result, the combined effect increases the critical heat flux. The mechanism associated in heat transfer during spray cooling has been explained with the help of a schematic diagram (Fig. 3.26).

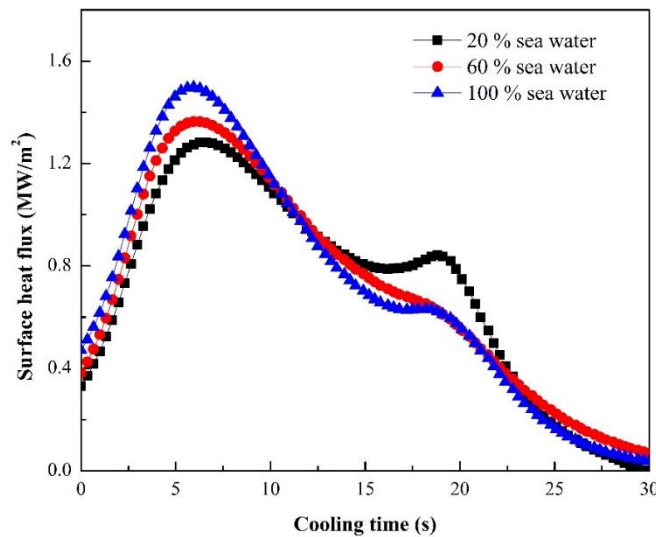


Fig. 3.25: Variation of surface heat flux with time

When the spray with sea water droplets on the hot surface, impinge on the hot plate discrete sites salt deposition occurs which prevent the film boiling effect by changing heat transfer mechanism from convective mode to conductive mode. In addition to the above due to surfactant effect of sea water, the droplet spreads more (Fig. 3.26b) in comparison to the pure salt case (Fig. 3.26a). The phenomena create more surface area when it touches the hot plate or the deposited salt. Fig. 3.27 shows boiling curve. All the boiling curves are showing the same trend.

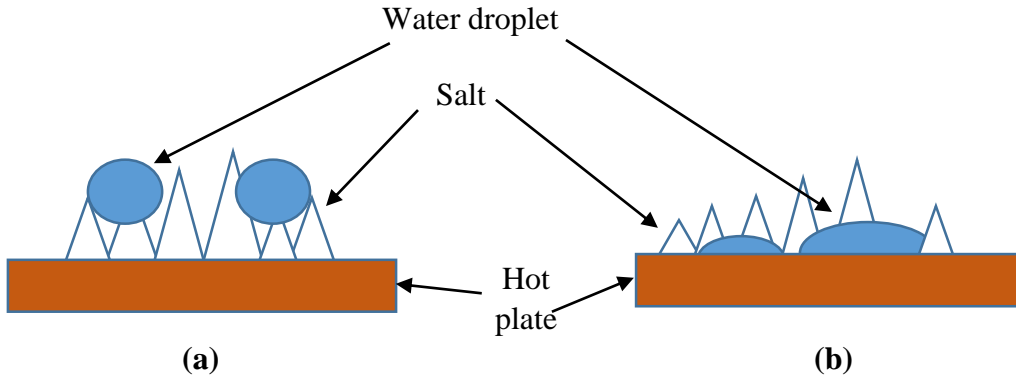


Fig. 3.26: Schematic diagram of spray cooling by (a) water with salt (b) sea water

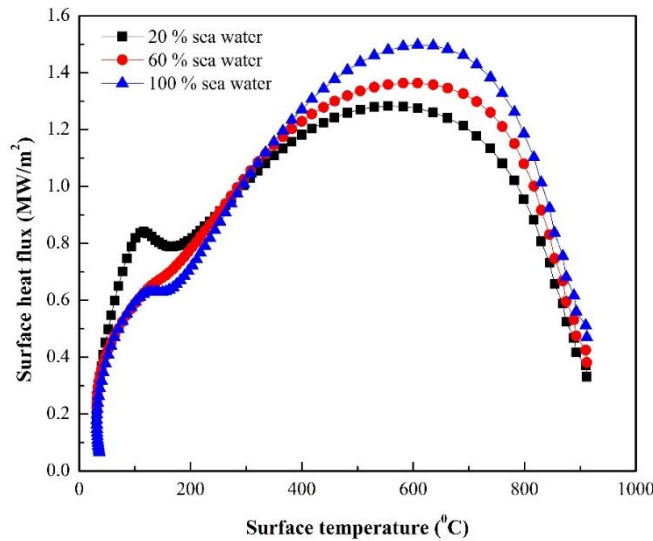


Fig. 3.27: Variation of surface heat flux with surface temperature

The average heat flux and the cooling rate with respect to time is calculated within the temperature range 900-600⁰ C which is shown in Fig. 3.28 and 3.29, respectively. Fig. 3.28 shows that by increasing sea water concentration average heat flux increases and gives a maximum value of 1.4 MW/m² at 100 % sea water concentration. Furthermore, from Fig. 3.29, it is also concluded that a maximum average cooling rate of 100 ⁰C/s is achieved in case of 100 % sea water.

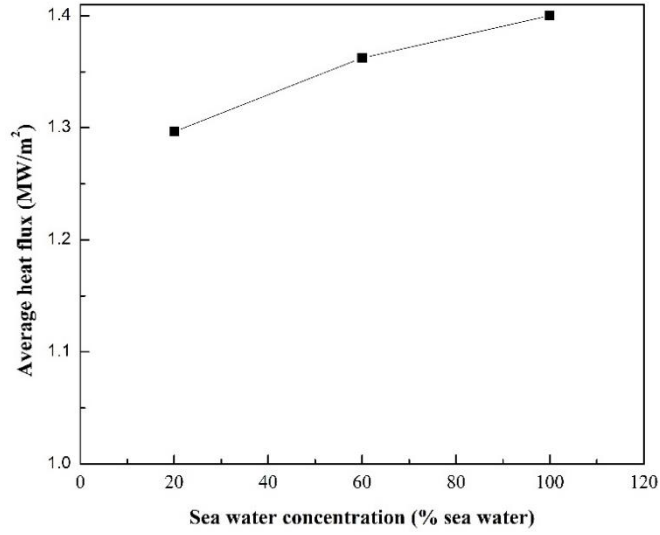


Fig. 3.28: Variation of average heat flux with sea water concentration

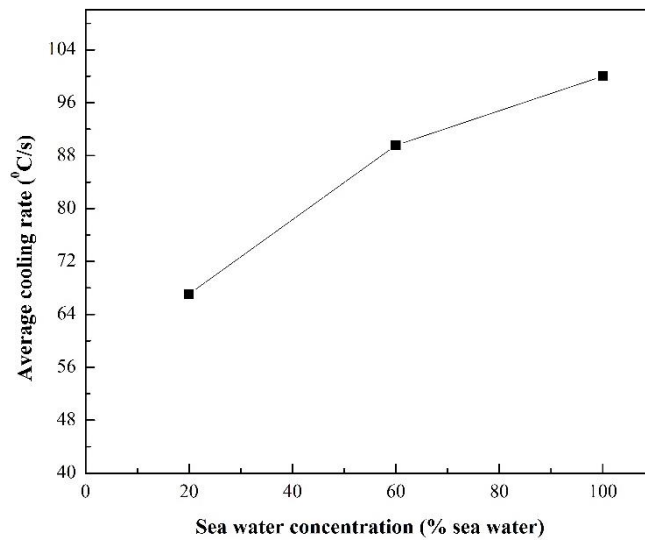


Fig. 3.29: Variation of average cooling rate with sea water concentration

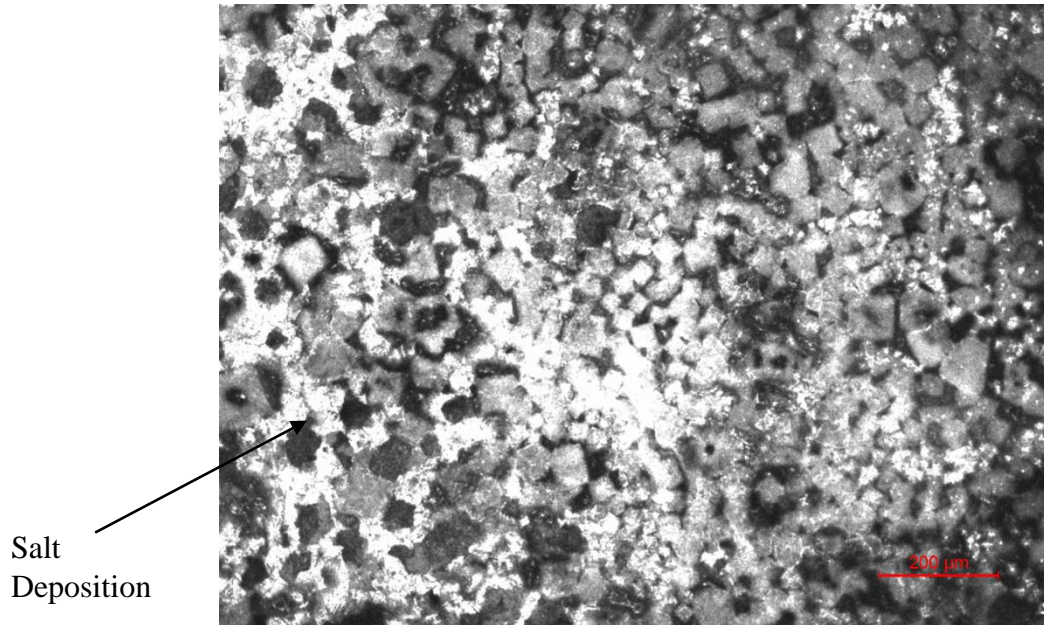


Fig. 3.30: Microscopic image of the steel plate after cooling with 100 % sea water

For the verification of heat transfer enhancement forced convection cooling zone or dark zone area (Fig. 3.31) were calculated from visual photograph (Fig. 3.32) and microscopic image (Fig. 3.30) taken to confirm the salt deposition. Both the aforesaid test confirms the heat removal rate during cooling.

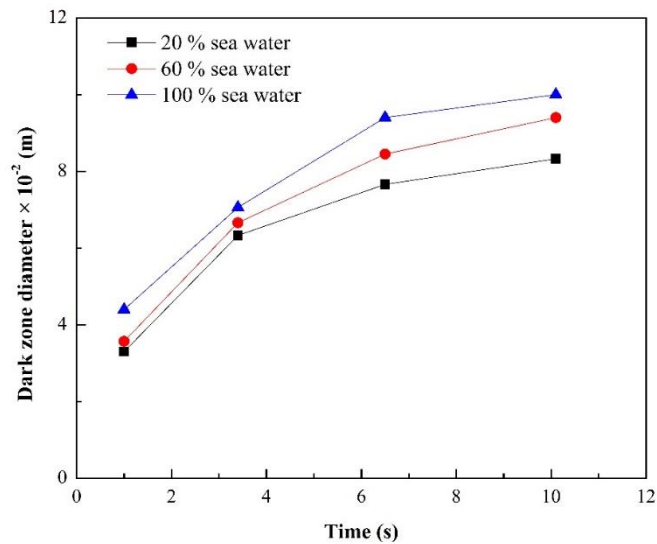


Fig. 3.31: Variation of dark zone diameter with time

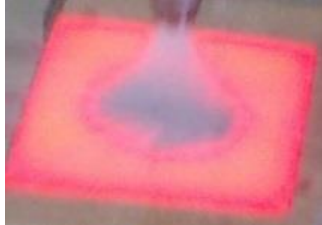

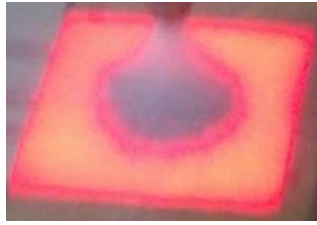









Sea water conc. (% sea water)			
Time (s)	20	60	100
0.1			
3.4			
6.5			
10.1			

Fig. 3.32: Visual analysis of experiments conducted with different concentration of sea water

3.5 Comparative study

The variation of surface heat flux with time of various type of coolant used are shown in the Fig. 3.33. All the curves are showing same trend. The maximum surface heat flux of 1.50 MW/m² is observed in case of 100 % sea water due to the presence of both the properties of salt and surfactant. In the other hand, salt + Tween 20 is showing a minimum value of surface heat flux due to presence of salt which reduce the foaming ability in the solution.

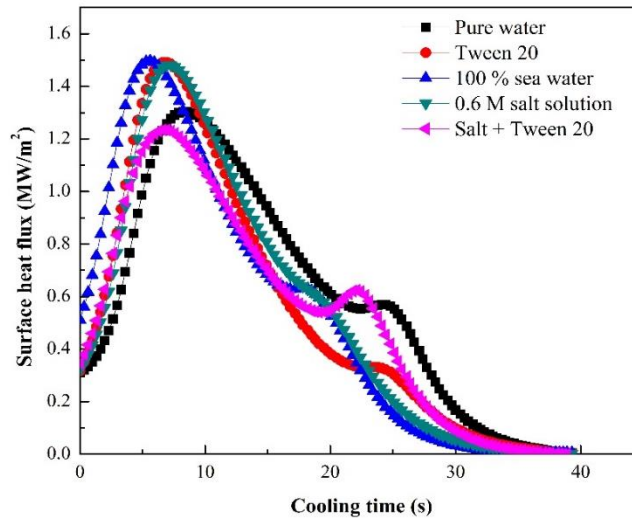


Fig. 3.33: Comparative study

3.6 Comparison with the previous work

In the absence of any results at high initial temperature (900⁰ C) and at very high mass flux, the current results are compared with results reported at similar conditions for the cooling methods such as air atomized spray. The current reported surface heat flux at different cooling rates are compared with work reported by Mohapatra et al. (2014). The comparison between the reported results and the current depicts some deviation which may be due to dissimilarity in cooling method used by the different researchers.

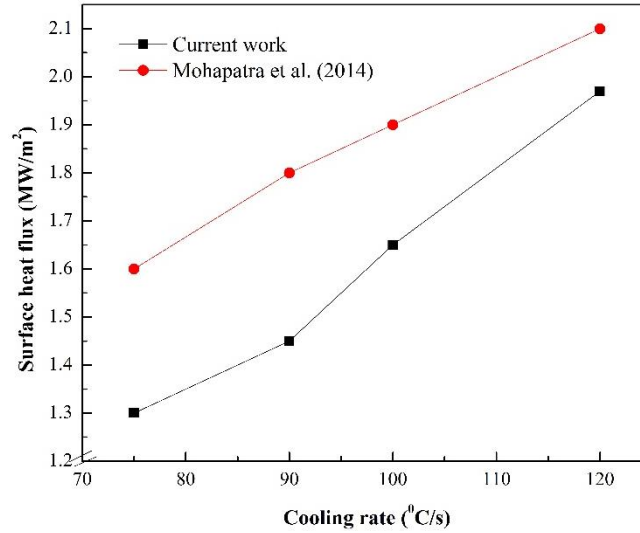


Fig. 3.34: Variation of surface heat flux with cooling rate

3.7 Validation

The time-temperature histories predicted by INTEMP software have been compared with the measured experimental results as shown in Fig. 3.35. In INTEMP software, node number 1715, 1765 and 1797 correspond to the thermocouples locations T/C1, T/C2 and T/C3 respectively. The close match between the measured and the predicted depicts the accuracy of the result. The maximum error calculated in between measured temperature and the estimated temperature is found to be less than 3 %.

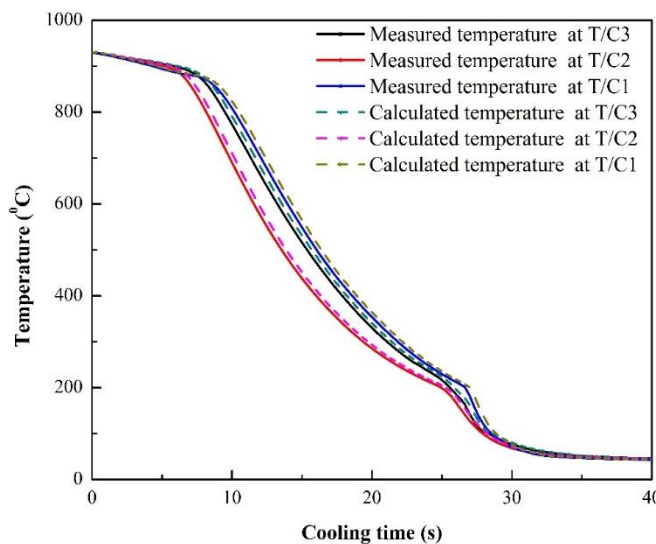


Fig. 3.35: Validation of estimated temperature with the measured

3.8 Measurement uncertainty

In the current study, the parameters to be varied are subsurface temperature, water flow rate and solution concentrations. The main source of uncertainty in subsurface temperature measurement are the exact location of the thermocouple and temperature fluctuation due to noise. For the accurate results, each experiments were conducted thrice and the average values are reported in the current work. From the average, a maximum $\pm 16\%$ deviation is noticed.

Chapter 4

Conclusions and future work

4.1 Conclusions

Based on the obtained results and corresponding discussions, the following are the current conclusions.

1. The optimum height for spray cooling is found to be 40 mm due to the dominance of average heat flux over spray area.
2. The optimum flow rate in the current case is $16.67 \times 10^{-5} \text{ m}^3/\text{s}$.
3. The salt added water spray reveals that the heat transfer rate increases with the increase in salt concentration up to 0.4 M due to the salt deposition effect and further increment of salt concentration decline the heat transfer rate due to decrement of net thermal conductivity and excessive salt deposition.
4. The surfactant added spray cooling reveals that the quenching rate enhance in the presence of surfactant in coolant.
5. The sea water spray cooling shows an increasing trend with the decreasing dilution by water. This happens because of the combined effect of salt deposition and contact angle decrement.
6. The comparative study discloses that the sea water spray cooling produces the maximum cooling rate.

4.2 Future work

The possible future works are as follows:

1. The spray cooling with sea water can be conducted from both the side of the plate.
2. All the cooling carried out in the current study can further be conducted in other cooling methodologies such as jet cooling and air atomized spray cooling.

References

- 1) Soumya S. Mohapatra, Satya V. Ravikumar, Ravi Ranjan, Surjya K. Pal, Shiv Brat Singh and Sudipto Chakraborty, Ultra-Fast Cooling and Its Effect on the Mechanical Properties of Steel Journal of Heat Transfer, vol. 136, pp. 1-9, 2014.
- 2) Rageey M.Youssef ,Modelling the effect of a spray on a liquid film on a heated surface, PhD Thesis, The College of Engineering and Mineral Resources, West Virginia,2007
- 3) Liu En-yang, Peng Liang-gui, Yuan Guo, Wang Zhao-dong, Zhang Dian-hua and Wang Guo-dong, Advanced run-out table cooling technology based on ultra-fast cooling and laminar cooling in hot strip mill, J. Cent. South University, vol. 19, pp. 1341-1345, 2012.
- 4) John D. Bernardin and Issam Mudawar, Film boiling heat transfer of droplet streams and sprays, Int. J. Heat Mass Transfer, vol. 40, pp. 2579-2593, 1997
- 5) Tadeusz Orzechowski and Sylwia Wcislik, Experimental analysis of the drop film boiling at ambient pressure, Energy Conversion and Management, vol. 76, pp. 918–924, 2013.
- 6) P. Bhattacharya, A.N. Samanta and S. Chakraborty, spray evaporative cooling to achieve ultra- fast cooling in runout table, Int. J. of Thermal Sciences, vol. 48, pp. 1741–1747, 2009.
- 7) Sugato Deb and S.C. Yao, Analysis on film boiling heat transfer of impacting sprays, Int. J Heat Mass Transfer, vol. 32, no. 11, pp. 2099-2112, 1989.
- 8) Matthew A. Clay and Michael J. Miksis, Effects of surfactant on droplet spreading, Physics of Fluids, vol. 16, No. 8, Pg. 3070-3078, 2004.
- 9) S. Chandra, M. di Marzo, Y. M. Qiao and P. Tartarini, Effect of Liquid-Solid contact angle on droplet evaporation, Fire Safety Journal, vol. 27, pp. 141-158, 1996.
- 10) A.I. Morgan, L. A. Bromely, C. R. Wilke, Effect of Surface Tension on heat Transfer in Boiling, Industrial and Engineering Chemistry Research. 41, 2767-2769, 1949
- 11) A.J. Lowery, J.W. Westwater, Heat Transfer to Boiling Methanol-Effect of Added agents, Industrial and Engineering Chemistry Research, 49, 1445-1448, 1957
- 12) P.D. Jonts, J. E. Myers, The Effect of Dynamic Surface Tension on Nucleate Boiling Coefficients, AIChE Journal, 6, 34-38, 1960
- 13) Y. M Qiao, S. M. Chandra, Spray Cooling Enhancement by Addition of Surfactant, Trans of ASME journal of Heat Transfer, 120, 92-98, 1998
- 14) M. Visaria, I. Mudawar, Effects of High Sub cooling on Two-Phase Spray Cooling and Critical Heat Flux, International Journal of Heat and Mass Transfer, 51, 5269-5278, 2008

- 15) U. Refiners, R. Jeschar, R. Scholoz, Heat Transfer during Continuous Casting Cooling because of Spray Water, *Steel Research*, 60, 442-450, 1989.
- 16) Q. Cui, S. Chandra, S. McCahan, The Effect of Dissolving Salts in Water Spray used for Quenching a Hot Surface: Part-1 Boiling of Single Droplets, *Trans Journal of Heat Transfer*, 125, 326-332, 2002.